International Forum on Aeroelasticity and Structural Dynamics
IFASD 2024
17-21 June 2024, The Hague, The Netherlands

NONLINEAR ANALYSIS OF COMBINED RATE AND ACCELERATION LIMITS EFFECT ON ACTUATOR PERFORMANCE

Luca Marino[1], **Xuerui Wang**[1], **Jurij Sodja**[1]

[1]Delft University of Technology
Kluyverweg 1, 2629HS Delft, The Netherlands
l.marino-1@tudelft.nl
x.wang-6@tudelft.nl
j.sodja@tudelft.nl

Keywords: Describing function, saturation regime, onset frequency, aeroservoelasticity, gust load alleviation

Abstract: This paper explores the nonlinear effects of rate and acceleration limits in actuation systems, focusing on the actuator steady-state response to sinusoidal input and the effectiveness of closed-loop control systems. The saturation regimes determined by rate and acceleration limits are investigated, and analytical formulations are derived for the nonlinear actuator response and the boundaries of these regimes within the two-dimensional parameter space defined by non-dimensional rate and acceleration limits. Describing functions for each regime are determined in a closed form, establishing the relationship between actuator input and output in the frequency domain. Combined rate and acceleration limits are found to induce a low-pass filter behaviour in the actuator, with a -40 dB/decade roll-off, and can lead to nonsmooth phase dependence on frequency. The describing functions of combined rate and acceleration limits are applied to the analysis of an aeroservoelastic wing model developed for gust load alleviation (GLA) purposes. The effect of the actuator limits is investigated by evaluating the onset point of the nonlinear behaviour and an equivalent describing function for the entire actuator-plant-control feedback loop. The resulting findings illustrate that rate and acceleration limits can substantially affect the performance of closed-loop systems, leading to phenomena such as jump resonances when partial-to-full saturation regime transitions occur, and thereby constraining the effective frequency range of the GLA control systems.

1 INTRODUCTION

In modern aircraft design, electro-mechanical actuators are increasingly being considered as an alternative to conventional hydraulic actuation systems for flight control surfaces. While offering advantages in terms of weight reduction and increased efficiency, these actuators are also characterised by a higher sensitivity to nonlinear effects. Unexpected nonlinear behaviour in actuators can strongly affect the effectiveness of control functions such as gust load alleviation or flutter suppression. Even more importantly, nonlinearities such as actuator rate limit can also generate dangerous phenomena, including pilot-induced oscillations [1]. Nonetheless, in state-of-the-art control law design and gust response analysis, actuator nonlinearities are often neglected [2] and linearised models with sufficiently high robustness margins are instead considered [3, 4]. Therefore, a deeper understanding of actuator nonlinearities is required to enhance their modelling and design, provide detailed certification guidelines, and determine under which conditions actuators can be operated safely and effectively.

This contribution focuses on the analysis of the nonlinear effects caused by rate and acceleration limits in the actuator response. The behaviour of rate-limited systems has been extensively investigated in the literature, particularly in response to the JAS39 Gripen [5] and YF-22 accidents [6], caused in the 90s by category II pilot-induced oscillations (PIO). Rate limit can occur in any actuation system due to its limited rate of travel. When the demanded velocity exceeds the rate limit, the actual actuator deflection will have a reduced amplitude and lag behind the input signal. This can either be caused by the input amplitude or frequency, rendering rate limit a frequency-dependent nonlinearity [2]. In hydraulic actuators, rate saturation occurs when the main control valve reaches its maximum flow capability [7]. Differently, in electro-mechanical actuators, achievable velocity is mostly determined by bearings and power limitations [2, 8]. In several applications, rate limit functions are also imposed in the control laws to limit the commanded actuator rate, aiming to protect the system from excessive commands and physical wear, and to avoid unwanted dynamic behaviour in the system's response [7, 9].

The theoretical analysis of rate-limited systems is often carried out by using sinusoidal describing functions. A describing function is an approximate frequency response function, which describes the relationship between the input and output of a nonlinearity in the frequency domain, and can be used to assess the effect of a single dominant nonlinearity, or a combination of nonlinearities, on the stability and robustness of a linear system [7, 10]. In closed-loop systems, describing functions are primarily used to determine the potential onset of limit cycle oscillations (LCOs); further applications include the prediction of subharmonics, jump phenomena, and the response of nonlinear systems to sinusoidal inputs [11]. As reported by Fielding and Flux [7], the main assumptions required for the validity of the describing function analysis are the time-invariance of the nonlinear element, and the presence of a dominant nonlinearity (or group of nonlinearities). In addition, the describing function is most effective when the linear element of the system does not present any high-frequency resonances which could cause the amplitudes of higher frequency harmonics to become significant. Nonlinearities such as rate and acceleration limits respect these assumptions, and increase the reliability of the analysis by acting as low-pass filters, therefore attenuating the high-frequency content of the linear element of the system.

The use of the describing function of the rate limit was first proposed by Hanke [12] for the analysis of the handling qualities of the open- and closed-loop systems in frequency domain, and the determination of the onset frequency of the rate limit nonlinearity from input amplitude and frequency. Describing function analysis was also used by Fielding and Flux [7] to investigate the stability and robustness of a closed-loop systems with a rate limiting element, with a particular focus on the prediction of LCOs induced by the nonlinearity in flight control systems. The prediction of the onset of category II PIO was addressed by several researchers, including Gilbreath [1] and Katayanagi [13]. In particular, Gilbreath derived an equivalent describing function able to describe the frequency response of closed-loop rate-limited systems, observing the presence of nonlinear jump resonances in the system's response and determining the open-loop onset point (OLOP) stability boundary, according to a procedure first introduced by Duda [14]. The describing function and the concept of open- and closed-loop onset frequency have also been used in many studies aimed at the design of rate limit compensation methods [9, 15–17].

While the rate limit nonlinearity has been studied by several authors, acceleration limit has only received little attention in the literature. In their investigation on the nonlinear behaviour of hydraulic actuation systems [7], Fielding and Flux concluded that acceleration limits should be

included in actuator models and that acceleration capability is an essential feature of actuation systems. Moreover, the describing function of fully saturated acceleration-limited systems was derived analytically and investigated, highlighting similar patterns to those already observed in rate-limited systems. More recently, Tang et al. [2, 8] investigated the effect of the actuator acceleration limit on the performance of closed-loop gust load alleviation aeroservoelastic systems. In this case, electro-mechanical actuators were considered and the acceleration limit was mainly due to maximum torque available in the system. Nonetheless, little is still known regarding the combined effects due to the simultaneous presence of actuator rate and acceleration limits, particularly when those nonlinearities only induce partial saturation in the output signal.

This paper presents an investigation into the combined nonlinear effects due to the presence of rate and acceleration limits in actuation systems. The saturation regimes determined by varying amount of these limits are analysed, and analytical formulations are derived for the boundaries corresponding to the transitions among different regimes. These boundaries are graphically represented in the two-dimensional parameter space determined by non-dimensional rate and acceleration limits parameters, dividing it into multiple regions corresponding to the different saturation regimes. Describing functions are analytically derived for all the saturation regimes defined by rate and acceleration limits, allowing for the investigation of their effect on the amplitude and phase of the steady-state actuator response in the frequency domain. Finally, the derived describing functions are used to investigate the effects of actuator rate and acceleration limits on the gust load alleviation performance of an aeroservoelastic system.

The paper is organised as follows. The investigation of the actuator saturation regimes under sinusoidal input is presented in Sect.2. In Sect.3, analytical describing functions are derived for rate and acceleration limits, and for combined rate and acceleration limit nonlinearities. The application of the describing functions to the analysis of a case-study aeroservoelastic system is addressed in Sect.4, while concluding remarks are provided in Sect.5.

2 ACTUATOR SATURATION REGIMES FOR SINUSOIDAL INPUT

This section presents the saturation regimes introduced by rate and acceleration limit in the steady-state actuator response to sinusoidal input. The boundaries associated with the transitions across different regimes are analytically derived, along with the response amplitude and phase delay for each saturation regime. Rate limit is discussed in subsection 2.1, acceleration limit is dealt within subsection 2.2, while the case of combined rate and acceleration limit is presented in subsection 2.3. An overview of the results, including the boundaries across different saturation regimes and their graphical representation in a two-dimensional parameter space, is achieved in subsection 2.4.

2.1 Rate limit

Let us first denote the actuator input and output signals as $x(t)$ and $y(t)$, respectively, and assume that a rate limit R_V is applied by the actuator on the output signal, such that

$$|\dot{y}(t)| \leq R_V. \tag{1}$$

If the signal

$$x(t) = x_0 \cos(\omega t) \tag{2}$$

is given as an input to the actuator, the rate limit will only be effective if the amplitude of the input rate exceeds R_V, i.e., if

$$R_V < \omega x_0; \tag{3}$$

otherwise, no saturation will occur and the output signal will be unaffected by the rate limit. In order to minimise the number of parameters needed to describe the rate limit effect on the actuator response, let us introduce the following non-dimensional time and signal amplitude:

$$\tau = \omega t \qquad\qquad \bar{x} = \frac{x}{x_0}. \tag{4}$$

In general, the notation $\bar{g}$ will be used to refer to a signal g normalised by the input amplitude, while the symbol ' will be used to indicate derivatives with respect to the non-dimensional time τ. The *rate limit ratio* can then be introduced as the ratio between the rate limit value and the maximum input rate

$$r_V = \frac{R_V}{\omega x_0} \tag{5}$$

such that the rate limit is only effective when $r_V < 1$.

When the rate limit is less than the maximum rate of the input signal, three different types of saturation regimes can occur in the steady-state actuator response, as shown in Fig.1: partial saturation without amplitude reduction (Fig.1a), partial saturation with amplitude reduction (Fig.1b) and full saturation (Fig.1c). These saturation regimes are analysed in what follows, focusing on the characterisation of regime transitions and on the evaluation of response amplitude and phase delay. In this paper, the expression *phase delay* will refer to the non-dimensional time interval between the maxima of the sinusoidal input ($\tau = 0$) and of the actuator steady-state response ($\tau = \phi$); in general, due to the response nonlinearity, this quantity will differ from the phase delay evaluated between their zeros or referred to the main harmonic component of the signals.

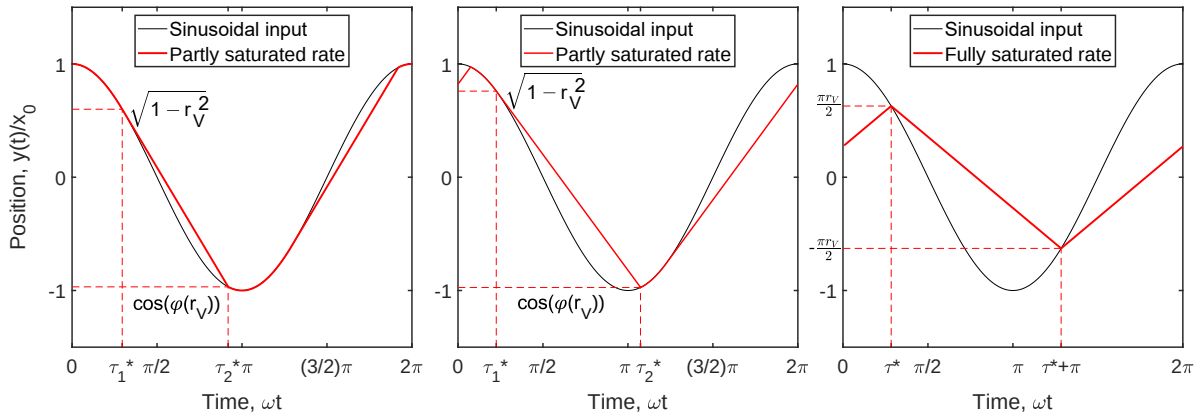

(a) $r_V = 0.8$ (b) $r_V = 0.65$ (c) $r_V = 0.4$

Figure 1: Steady-state response of a rate-limited actuator to sinusoidal input.

Partial saturation with no amplitude reduction (Fig.1a) is the first regime observed as the rate limit ratio is decreased below unity. In this regime, the time interval where saturation occurs is entirely included within the half-period between a maximum and the subsequent minimum of the sinusoidal input, and therefore the maximum value of the steady-state response remains unaltered and no phase delay is observed, as also reported by Yuan et al. [9]. The non-dimensional time τ_1^* where saturation first occurs in the interval $\tau \in [0, 2\pi]$ can easily be determined as the time instant where the input velocity $\bar{x}' = -\sin(\tau)$ equates the rate limit ratio r_V, and is therefore given by

$$\tau_1^* = \sin^{-1}(r_V), \tag{6}$$

while the corresponding response value is

$$\bar{y}_1^* = \sqrt{1 - r_V^2}. \tag{7}$$

As visible in Fig.1a, output saturation terminates when the rate limited output intersects the sinusoidal input, at $\tau = \tau_2^*$. Let us introduce the function φ of the rate limit ratio such that $\tau_2^* = \varphi(r_V)$ and $\bar{x}_2^* = \cos(\varphi(r_V))$. Evaluating the intersection between the linear portion of the actuator output, whose equation reads as

$$\bar{y}(\tau) = \sqrt{1 - r_V^2} - r_V(\tau - \tau_1^*), \tag{8}$$

and the input signal $\bar{x}(\tau) = \cos(\tau)$, it is possible to obtain the following implicit analytical expression for $\varphi(r_V)$:

$$r_V \varphi(r_V) + \cos(\varphi(r_V)) = r_V \sin^{-1}(r_V) + \sqrt{1 - r_V^2}. \tag{9}$$

A graphical representation of the function $\varphi(r_V)$ is provided in Fig.2. As it is possible to observe in Fig.2, $\varphi(r_V)$ is a monotonically decreasing function of r_V, whose minimum value is $\pi/2$ at $r_V = 1$.

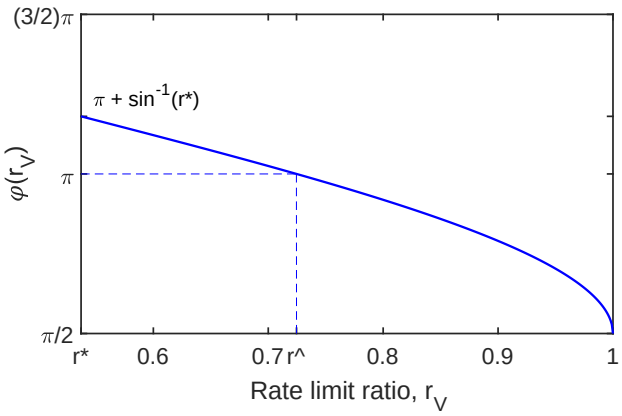

Figure 2: Non-dimensional ending saturation time in partial rate saturation regime as a function of the rate limit ratio.

If the saturation ending time is such that $\tau_2^* > \pi$, the maxima of the sinusoidal input will also be saturated, leading to a reduction of amplitude and a non-zero phase delay in the actuator output (Fig.1b). The rate limit ratio value $r^\wedge$ at the regime transition between these saturation regimes can be determined numerically by solving the equation $\phi(r_V) = \pi$, and is equal to 0.7246. In this further regime, named as partial saturation with amplitude reduction, the amplitude of the actuator steady-state response will be equal to $-\cos(\varphi(r_V))$ and the phase delay will be $\phi = \varphi(r_V) - \pi$.

The transition from partial to full rate saturation occurs when the ending time of the saturation interval τ_2^* coincides with the start of the subsequent saturation interval at $\tau_1^* + \pi$, i.e., when

$$\varphi(r_V) = \pi + \sin^{-1}(r_V). \tag{10}$$

This leads to rate saturation occurring throughout the entire period of the steady-state response. By replacing the above value of $\varphi(r_V)$ into Eq.(9), it is obtained that the transition takes place when the rate limit ratio is equal to

$$r^* = \frac{2}{\sqrt{4 + \pi^2}} \cong 0.5370, \tag{11}$$

as already observed by several authors (see, e.g., [1, 14]).

The actuator output in full rate saturation regime is characterised by a sequence of linear variations of the position over time (see Fig.1c), with non-dimensional rate remaining constant at $\pm r_V$; the output signal therefore resembles a triangle wave. Given the 2π-periodicity of the response and its rate, it is easily obtained that the signal amplitude in this regime is equal to $(\pi/2)r_V$, while the non-dimensional time of the maximum positive output within the interval $[0, 2\pi]$, representing the phase delay, is

$$\phi = \tau^* = \cos^{-1}\left(\frac{\pi}{2} r_V\right), \tag{12}$$

since the switching between the positive and negative saturated rate occurs across the intersection with the sinusoidal input.

The amplitude and phase delay of the steady-state response, evaluated across the different saturation regimes, are represented in Figs.3a and b, respectively. It is possible to note that, while only a limited amplitude reduction (up to about 15%) is observed in partial saturation regimes, the response amplitude decreases linearly in full saturation regime, approaching zero as $r_V \to 0$. Differently, the phase delay gradually increases as the rate limit ratio is decreased below the value $r^\wedge$, maintaining a similar behaviour across partial and full saturation regimes and eventually tending to $\pi/2$ when $r_V \to 0$.

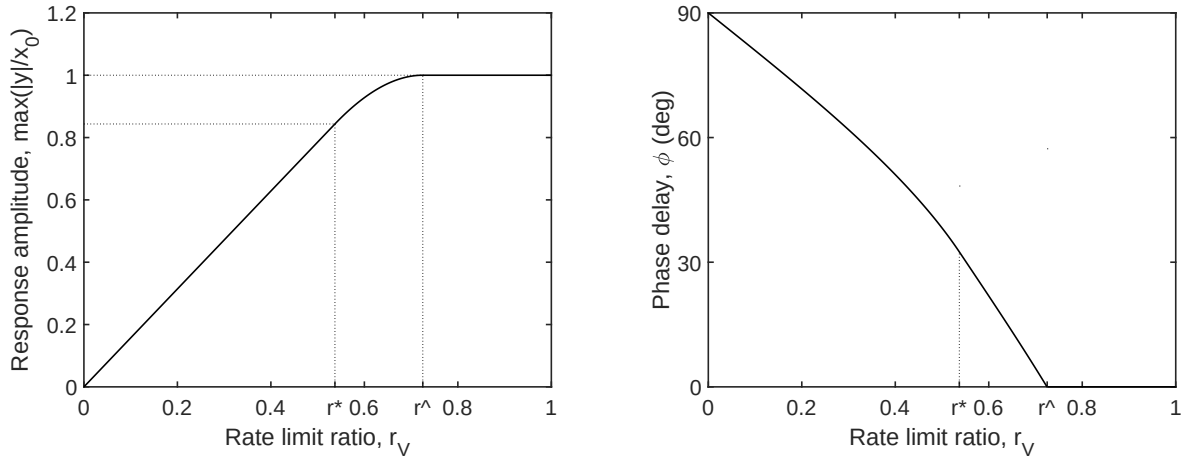

(a) (b)

Figure 3: Non-dimensional response amplitude (**a**) and phase delay (**b**) of the steady-state actuator response for varying rate limit ratio.

2.2 Acceleration limit

Let us now analyse the effect of the acceleration limit R_A, such that

$$|\ddot{y}(t)| \leq R_A, \tag{13}$$

on the actuator output in steady-state conditions, in the assumption that no rate limit is applied by the actuator. Since the maximum input acceleration of the sinusoidal signal from Eq.(2) is equal to $\omega^2 x_0$, it is convenient to introduce the *acceleration limit ratio* as

$$r_A = \frac{R_A}{\omega^2 x_0}. \tag{14}$$

In this notation, the acceleration limit will only affect the actuator output if $r_A < 1$. In this case, three saturation regimes can be observed: partial saturation without (Fig.4a) or with velocity reduction (Fig.4b) and full saturation (Fig.4c). It can be observed that the effect of the acceleration limit on the output velocity is the same as that of the rate limit on the output position. However, this leads to a significantly different actuator output from that induced by the rate limit, as shown in Fig.5 for the three saturation regimes and discussed in what follows.

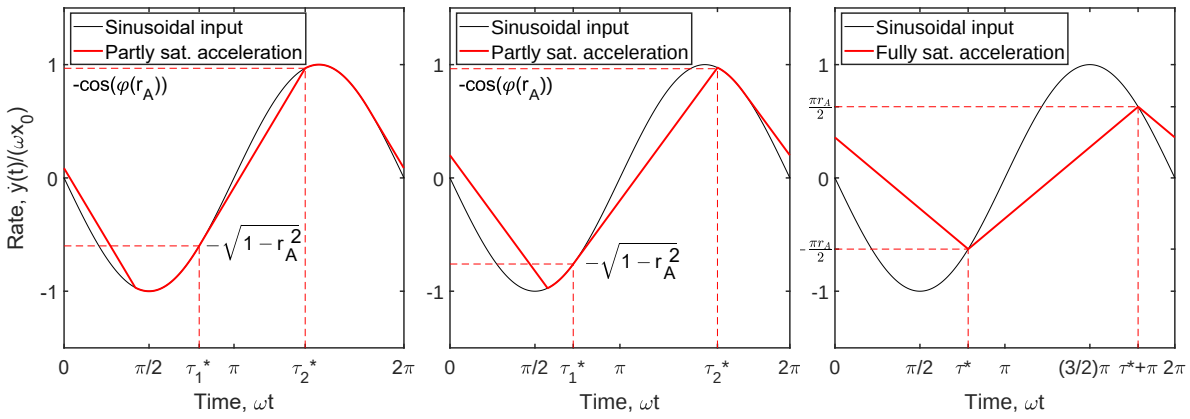

(a) $r_A = 0.8$ (b) $r_A = 0.65$ (c) $r_A = 0.4$

Figure 4: Steady-state output rate of an acceleration-limited actuator under sinusoidal input.

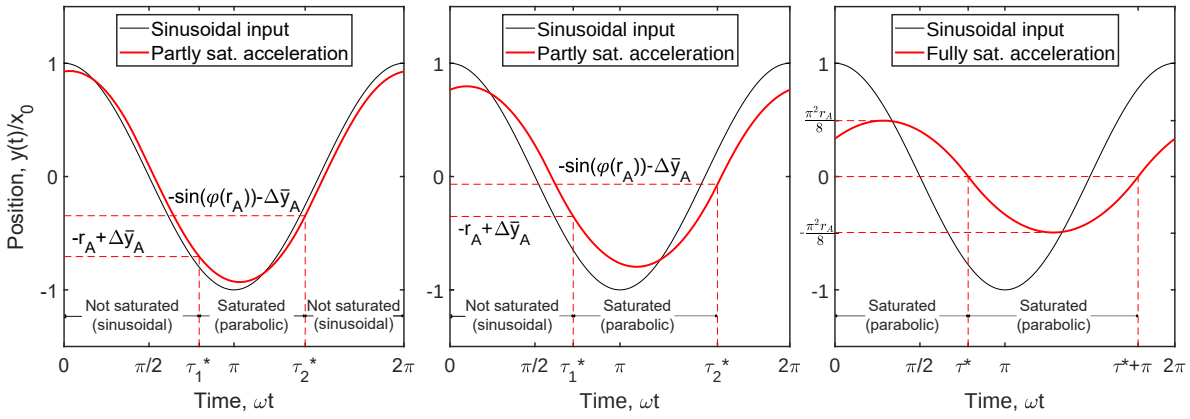

(a) $r_A = 0.8$ (b) $r_A = 0.65$ (c) $r_A = 0.4$

Figure 5: Steady-state output position of an acceleration-limited actuator under sinusoidal input.

In partial acceleration saturation regimes, the actuator steady-state response presents a parabolic evolution in those time intervals where the acceleration is saturated. The output position therefore consists in a sequence of sinusoidal and parabolic traits (see, e.g., Fig.5a). Since the maximum acceleration in the sinusoidal input occurs in correspondence of the maximum deflection (in absolute value), amplitude reduction is observed in the actuator output for any acceleration limit such that $r_A < 1$. Therefore, unlike rate limit, acceleration limit cannot lead to partial saturation regime with no amplitude reduction. By extending the results shown in subsection 2.1 to the acceleration limit case, it can easily be derived that the starting and ending times of the saturation interval are $\tau_1^* = \varphi(r_A) - \pi/2$ and $\tau_2^* = \cos^{-1}(-r_A)$. Another noteworthy effect of the acceleration limit is that, differently from rate limit, it also induces a phase delay in the sinusoidal traits of the output signal, i.e., in those time intervals where the acceleration is not saturated. This behaviour can be explained by observing, for instance, Fig.6a. During

the saturation interval $[\tau_1^*, \tau_2^*]$, the absolute variation of the parabolic output is smaller than that of the underlying sinusoidal input by a quantity equal to $2\Delta\bar{y}_A$, due to the smaller curvature imposed by the acceleration limit. Denoting with $\Delta\tau_A = \tau_2^* - \tau_1^*$ the saturation time interval, it is possible to derive an analytical formulation of $\Delta\bar{y}_A$ as

$$\Delta\bar{y}_A = \frac{1}{2}\left[r_A + \sqrt{1 - r_A^2}\Delta\tau_A - \frac{1}{2}r_A\Delta\tau_A^2 - \sin(\varphi(r_A))\right]. \tag{15}$$

The evolution of $\Delta\bar{y}_A$ with respect to the acceleration limit ratio in partial saturation regime is reported in Fig.6b, where it is possible to observe its gradual increase from zero to r^* as r_A is decreased from 1 to r^*. $\Delta\bar{y}_A$. Once $\Delta\bar{y}_A$ has been evaluated, the response amplitude and phase delay can simply be derived by exploiting the mathematical properties of parabolas. After some algebraic calculations, the resulting values are

$$\max_{[0,2\pi]} |\bar{y}| = \frac{1 + r_A^2}{2r_A} - \Delta\bar{y}_A \tag{16}$$

and

$$\phi = \frac{\sqrt{1 - r_A^2}}{r_A} - \cos^{-1}(r_A) \tag{17}$$

respectively.

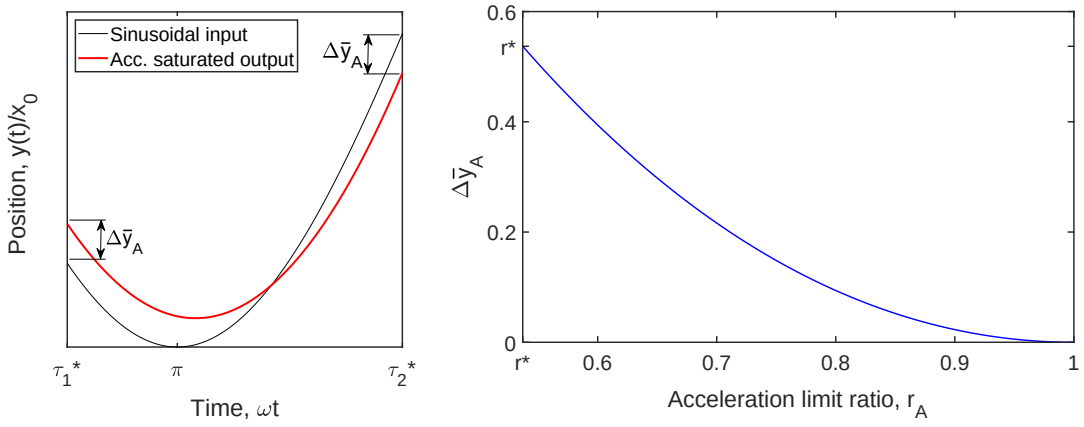

(a) (b)

Figure 6: (**a**) Generation of an offset $\pm\Delta\bar{y}_A$ between input and output during acceleration saturated intervals in partial saturation regime and (**b**) evolution of $\Delta\bar{y}_A$ for varying acceleration limit ratio.

In full acceleration saturation regimes, the steady-state actuator response consists in a sequence of parabolic traits, as shown in Fig.5c, corresponding to the acceleration switching between r_A and $-r_A$. Exploiting the properties of parabolas and the response symmetry, it can be derived that, in this case, the response amplitude is equal to $(\pi^2/8)r_A$, while the phase delay is given by $\phi = \cos^{-1}(r_A)$.

Amplitude and phase delay of the steady-state response are finally plotted in Fig.7 across all saturation regimes for acceleration limited signals. By comparing these plots with Figs.3a and b, depicting the same quantities for rate limited signals, it is possible to observe that the main difference is that both response amplitude and phase delay are also affected by the saturation for $r^\wedge \leq r_A < 1$. In the remaining saturation regimes, the response amplitude decreases to zero at a slower rate than in the rate limit case, while the phase delay follows the same pattern in full saturation regime, tending to $\phi = \pi/2$ when $r_A \to 0$.

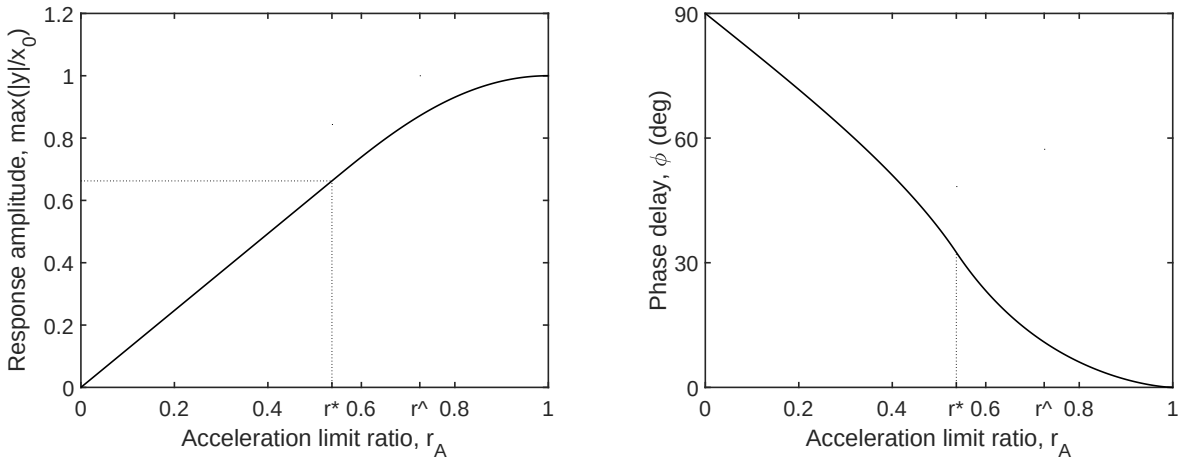

(a) (b)

Figure 7: Non-dimensional response amplitude (**a**) and phase delay (**b**) of the steady-state actuator response for varying acceleration limit ratio.

2.3 Combined rate and acceleration limit

Let us consider the case of an actuator where the output signal rate and acceleration are limited by R_V and R_A respectively. As discussed in Sect. 1, the presence of combined rate and acceleration limits can be the consequence of physical limitations, including limited power and torque available, or it can be imposed by ad-hoc filters (see, e.g, [18, 19]) to prevent the actuator from excessive commanded output which could lead to physical damage. It is important to consider that, when rate saturation occurs, the output rate of the actuator becomes nonsmooth (see Fig.3), leading to the presence infinitely large spikes in the output acceleration in correspondence of the transition times τ_1^*, τ_2^* and τ^* . As a consequence, any finite value of the acceleration limit will affect the actuator output. Conversely, no effects from the rate limit will be seen when $r_V \geq 1$; in this case, the output signal will behave as described in subsection 2.2. Actuator behaviours for $r_V < 1$ are addressed in following discussion, which is organised by considering three different configurations: (i) full rate saturation ($r_V \leq r^*$) with any acceleration limit; (ii) partial rate saturation ($r^* < r_V < 1$) with acceleration limit $r_A \geq 1$; (iii) partial rate saturation with acceleration limit $r_A < 1$. Transitions among the different saturation regimes, response amplitude and phase delay will be derived and represented in the two-dimensional parameter space defined by r_V and r_A.

2.3.1 Full rate saturation with acceleration limit

In this first case, it is assumed that an acceleration limit is applied along with a rate limit such that $r_V \leq r^*$. In this scenario, the rate limit leads to full saturation, independently of the acceleration limit value; therefore, partial saturation is not possible under any circumstances. However, the instantaneous switching between positive and negative rate saturation, represented in Fig.1c, leads to the presence of discontinuities in the output signal rate, and to infinitely large acceleration peaks. As a consequence, any finite value of the acceleration limit will affect the signal, eliminating discontinuities in the output rate. Therefore, two different saturation regimes are possible: full mixed saturation, where an alternation of rate and acceleration saturated intervals occurs (see Fig.8a), or full acceleration saturation only, where no rate saturation is observed, as shown in Fig.8b.

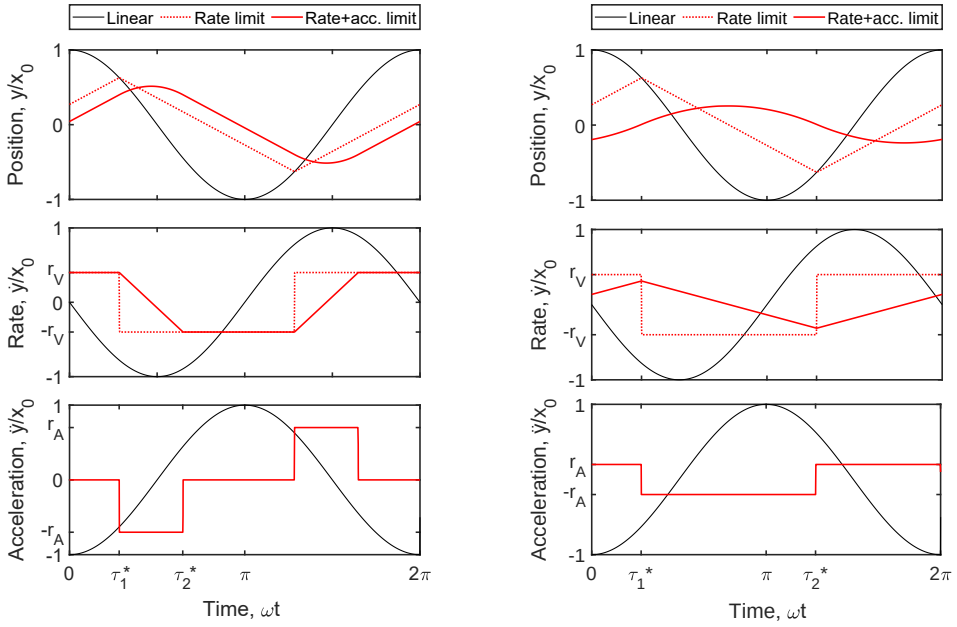

(a) $r_A = 0.4$ (b) $r_A = 0.2$

Figure 8: Steady-state response of a rate and acceleration-limited actuator to sinusoidal input for $r_V = 0.4$.

Full mixed saturation results from the saturation of the acceleration peaks generated by the rate discontinuities. In Fig.8a, it can be observed that the acceleration saturation interval starts in correspondence of the switch between positive and negative rate saturation, at $\tau_1^* = \cos^{-1}((\pi/2)r_V)$. The ending time of this saturation can be determined by observing the output rate patterns. In fact, considering the acceleration saturation interval starting at τ_1^*, where $\bar{y}'(\tau_1^*) = r_V$, it can be noted that the ending time τ_2^* corresponds to the intersection between the linear rate variation determined by the acceleration limit and the subsequent negative rate saturation, so that $\bar{y}'(\tau_2^*) = -r_V$. Denoting with $\Delta\tau_A$ the time duration of the acceleration saturation interval, it can be easily deduced that

$$\Delta\tau_A = \frac{2r_V}{r_A}. \tag{18}$$

The produced output velocity consists in a trapezoidal wave, oscillating between $\pm r_V$ with slope given by $\pm r_A$, while the position presents an alternation of linear and parabolic traits. In particular, the linear traits of the actuator response are delayed by r_V/r_A with respect to those obtained if only the rate limit is considered. The response amplitude coincides with maximum of the parabolic traits, which is

$$\max_{[0,2\pi]} |\bar{y}| = \frac{1}{2} r_V \left(\pi - \frac{r_V}{r_A}\right) \tag{19}$$

and occurs at the time:

$$\phi = \cos^{-1}\left(\frac{\pi}{2} r_V\right) + \frac{r_V}{r_A}. \tag{20}$$

The transition to fully saturated acceleration regime takes place when the value of r_A is such that acceleration is saturated in the whole interval $[\tau_1^*, \tau_2^*]$, i.e., for

$$r_A = \frac{2}{\pi} r_V. \tag{21}$$

In fact, in this case, the acceleration saturation interval becomes $\Delta\tau_A = \pi$, covering half of the signal period. Further decreasing of r_A will only lead to an amplitude reduction of the output, which will be equal to $(\pi/2)r_A$, as specified in subsection 2.2. However, since the switch between positive and negative acceleration saturation occurs in correspondence of the saturation switching in the underlying rate limited signal (see Fig.8b), the phase delay will be

$$\phi = \pi - \sin^{-1}\left(\frac{\pi}{2} r_V\right). \tag{22}$$

It is noteworthy to underline that, while a strict acceleration limit can conceal the presence of a rate limit, which does not affect the response amplitude in this saturation regime, the effect from the latter can still be observed in terms of phase delay in the output signal, which is, in this specific case, only dependent on the rate limit ratio.

2.3.2 Partial rate saturation with acceleration limit $r_A \geq 1$

The saturation regime scenario is more complex for those signals whose rate limit ratio is included in the range between r^* and 1. In this case, the acceleration limit can affect the actuator output in two different ways: for $r_A \geq 1$, its effect is still limited to the saturation of the acceleration peaks generated by the discontinuities in the output rate; differently, for $r_A < 1$, acceleration saturation also occurs in the sinusoidal traits of the steady-state response. The first case is dealt with in this subsection, while the second case will be discussed in subsection 2.3.3.

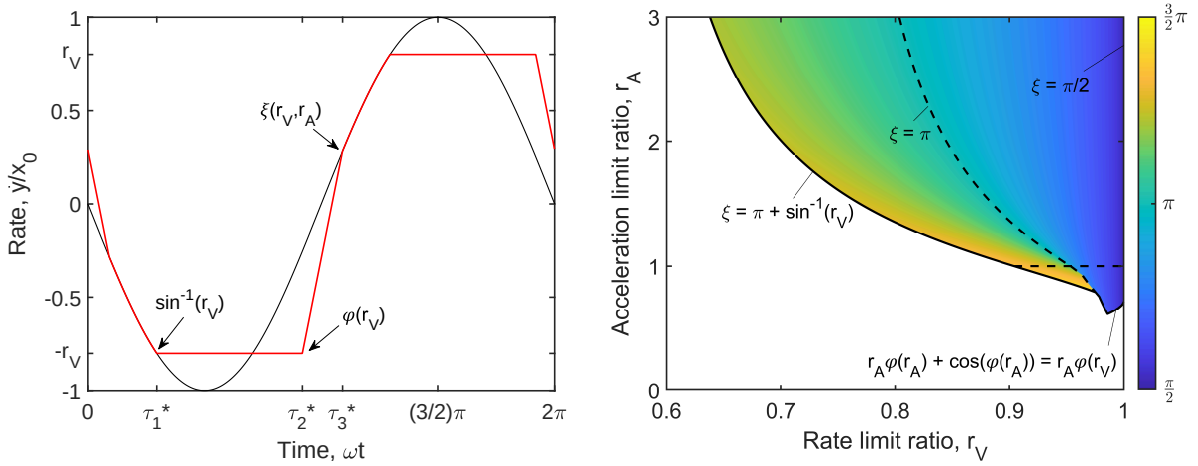

(a) (b)

Figure 9: (**a**) Steady-state output rate of a rate- and acceleration-limited actuator under sinusoidal input for $r_V = 0.8$ and $r_A = 2$ and (**b**) evolution of the non-dimensional ending time of the acceleration saturation interval in mixed partial saturation regime.

An example of the effect of the combined rate and acceleration limit for $r^* < r_V < 1$ and $r_A \geq 1$ is provided in Fig.9a, where the actuator output rate is shown for $r_V = 0.8$ and $r_A = 2$ It is possible to observe how the acceleration limit is activated by the discontinuity generated by the rate limit at $\tau = \varphi(r_V)$, leading to an acceleration saturation (shown by the linear variation of the rate) between this point and the subsequent intersection with the sinusoidal input. Let us denote the non-dimensional ending time of the acceleration saturation as ξ, which is defined by the implicit equation

$$r_A(\xi - \varphi(r_V)) + \sin\xi = r_V. \tag{23}$$

The evolution of ξ with r_V and r_A is graphically represented in Fig.9b. Limiting the present discussion to the case $r_A \geq 1$, it is possible to observe the minimum value of ξ is $\pi/2$ when

$r_V = 1$, i.e., when no rate saturation occurs, while $\xi \to \varphi(r_V)$ when $r_A \to \infty$. In general, ξ increases for decreasing rate limit ratios (due to the increase of $\varphi(r_V)$) and for decreasing acceleration limit ratios, due to the increased duration of the acceleration saturation interval.

Three types of steady-state response are possible in this region of the parameter space $r_V - r_A$, as shown in Fig.10 for $r_A = 2$ and varying r_V. When $\xi \leq \pi$, the acceleration saturation terminates with the first half of the response period and the maximum output is still observed in the sinusoidal trait, at $\tau = 0$. In this regime, which can be referred to as *mixed partial saturation*, the sinusoidal traits of the steady-state response present an offset with respect to the sinusoidal input, similarly to that observed in partly saturated acceleration regime in subsection 2.2. In this case, adopting the same reasoning discussed above and illustrated in Fig.6a, it is derived that this offset $\Delta\bar{y}_{VA}$ is equal to

$$\Delta\bar{y}_{VA} = \frac{1}{2}\left[\cos\xi - \cos(\varphi(r_V)) + r_V\Delta\tau_{VA} - \frac{1}{2}r_A\Delta\tau_A^2\right], \tag{24}$$

where

$$\Delta\tau_{VA} = \xi - \varphi(r_V). \tag{25}$$

is the duration of the acceleration saturation interval. Consequently, it can be concluded that the maximum response in the case represented in Fig.10a, is equal to $1 + \Delta\bar{y}_{VA}$. It is noteworthy how the combined rate and acceleration limit leads, in this case, to a slight increase of the actuator output, compared to the linear case.

When $\xi > \pi$ (See Fig.10b), even though mixed partial saturation still occurs, different properties are observed in the actuator response. Since the acceleration saturation ends after $\tau = \pi$, the response maximum is observed within the saturated interval, i.e., in the parabolic trait of the response. It can be derived that, in this region of the parameter space, the response amplitude is equal to

$$\max_{[0,2\pi]} |\bar{y}| = \frac{r_V^2}{2r_A} - \cos(\varphi(r_V)) - \Delta\bar{y}_{VA}, \tag{26}$$

while the phase delay is now given by

$$\phi = \varphi(r_V) + \frac{r_V^2}{2r_A} - \pi. \tag{27}$$

Finally, a transition to full mixed saturation regime (Fig.10c) is observed when the acceleration saturation covers the whole interval between the end of the first rate saturation and the start of the subsequent rate saturation, i.e., when $\xi = \pi + \sin^{-1}(r_V)$. By substituting this value into Eq.(23), it is obtained that the boundary between full and partial mixed saturation regimes can written as

$$r_A = \frac{2r_V}{\pi + \sin^{-1}(r_V) - \varphi(r_V)}. \tag{28}$$

In full mixed saturation regime, the amplitude steady-state response can still be obtained from Eq.(19), while the phase delay will differ from that provided by Eq.(20), assuming instead the value given by Eq.(27).

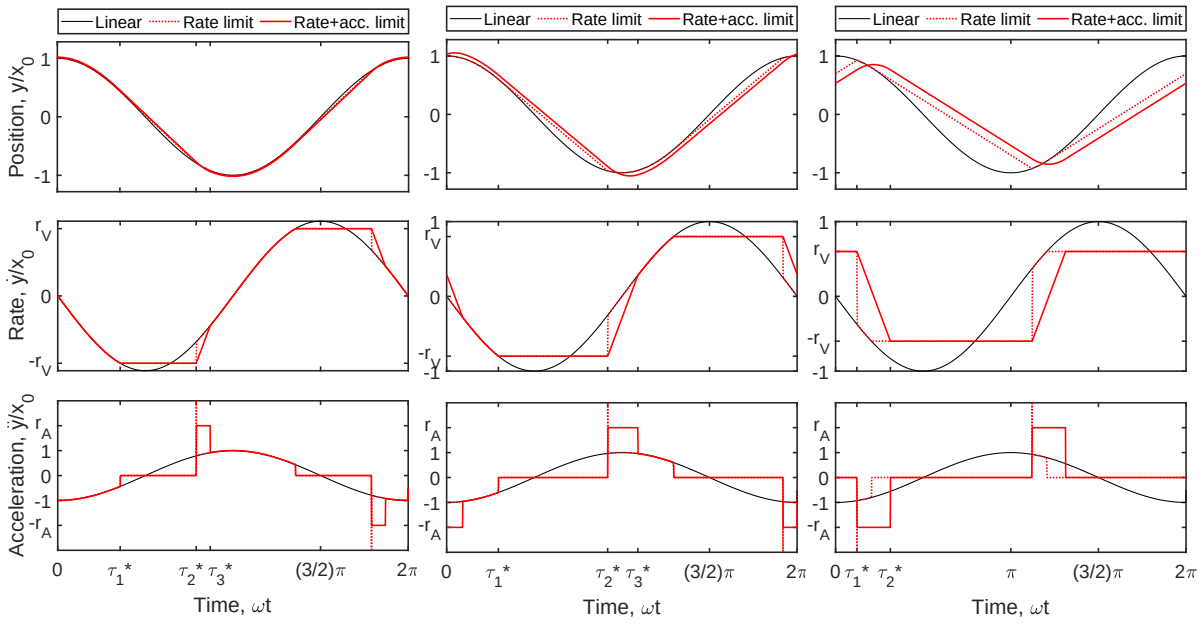

(a) $r_V = 0.9$ (b) $r_V = 0.8$ (c) $r_V = 0.6$

Figure 10: Steady-state response of a rate- and acceleration-limited actuator to sinusoidal input for $r_A = 2$.

2.3.3 Partial rate saturation with acceleration limit $r_A < 1$

In the region of the parameter space characterised by $r^* < r_V < 1$ and $r_A < 1$, the acceleration limit can saturate not only the spikes generated by discontinuities in the output rate, but also the sinusoidal traits of the signal, leading to a complex scenario in terms of possible saturation regimes. In general, it can be stated that:

- acceleration peak saturation occurs between $\tau = \varphi(r_V)$ and $\tau = \xi$;
- acceleration sine saturation occurs between $\tau = \cos^{-1}(r_A)$ and $\tau = \varphi(r_A) + \pi/2$, as shown in subsection 2.2.

In the context of mixed partial saturation, this can lead to two different actuator responses. From Fig.9b, it can be observed that, when $r_A < 1$, a jump discontinuity occurs across the line $\xi = \pi$. In particular, it is found that, moving across such a line (in the direction of increasing r_V), the value of ξ has a sharp drop from $\varphi(r_A) + \pi/2$ to $\cos^{-1}(r_A)$. Therefore, when $\xi > \pi$, the sine saturation time interval is fully included in the peak saturation interval, so that only the latter is observed. As shown in Fig.11a, the resulting output signal presents the same properties already discussed in the previous subsection for the case $r_A \geq 1$ for $\xi > \pi$ (see Eqs.(26) and (27)). Differently, when $\xi < \pi$, two distinct acceleration saturation intervals are observed (see in Fig.11b). This leads to a third type of mixed partial saturation regime, with different properties from those discussed above. In particular, since the maximum occurs during the acceleration sine saturation, the phase delay will be the same determined for the partial acceleration saturation case in Eq.(17). The response amplitude, consistently with the formulations derived for mixed partial saturation (case $r_A \geq 1$, $\xi \leq \pi$) and partly saturated acceleration (see Eq.(16)), is given by

$$\max_{[0,2\pi]} |\bar{y}| = \frac{1 + r_A^2}{2r_A} - \Delta\bar{y}_A + \Delta\bar{y}_{VA}. \tag{29}$$

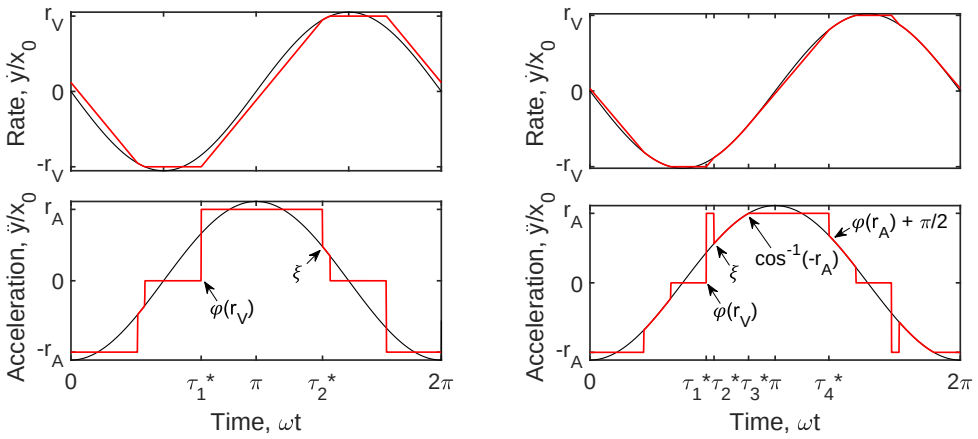

(a) $r_V = 0.95$ (b) $r_V = 0.98$

Figure 11: Steady-state response of a rate- and acceleration-limited actuator to sinusoidal input for $r_A = 0.9$.

The regime transition from mixed partial saturation with $\xi > \pi$ to mixed full saturation occurs across the boundary indicated by Eq.(28), as already discussed for $r_A \geq 1$. The remaining regime transitions are represented in Fig.12a and discussed in what follows.

- The transition from mixed partial saturation with $\xi < \pi$ to full mixed saturation simply occurs across the line $\xi = \pi$, after this intersects with the boundary from Eq.(28).
- For $r_A \leq r^{\wedge}$, mixed partial saturation ($\xi < \pi$) can also transition to a partly saturated acceleration regime. This transition occurs when the rate limit value is no longer reached in the rate output (see the case $r_V = 0.99$ in Fig.12b). The boundary can be implicitly formulated as

$$r_A \left(\varphi(r_A) - \varphi(r_V) + \frac{\pi}{2} \right) + \cos(\varphi(r_A)) = r_V. \tag{30}$$

- Also for $r_V < 1$, the final transition from partial to full acceleration saturation occurs at $r_A = r^*$. However, transitions can also take place for larger values of r_A, as graphically explained in Fig12b. Let us consider the case $r_V = 0.97$. As r_A is progressively decreased, the saturation regimes transition first to mixed full saturation across the boundary $\xi = \pi$, then to full acceleration saturation across the boundary from Eq.(21). A further transition to partly saturated acceleration occurs when the linear trait of the saturated output is such to intersect the sinusoidal input. The boundary corresponding to this regime transition can be implicitly expressed as

$$r_A \left(\varphi(r_A) - \varphi(r_V) \right) + \cos(\varphi(r_A)) = 0. \tag{31}$$

While the full acceleration saturation regime has already been characterised in subsection 2.2, it has also been shown that the phase delay can assume different values depending on the considered region in the parameter space $r_V - r_A$. For $r^* < r_V < 1$, two different behaviours are possible, as shown in Fig.13:

- if the switch between the positive and negative saturated traits occurs across the sinusoidal input, the presence of a rate limit is irrelevant and the phase delay will be $\phi = \cos^{-1}(r_A)$, as detailed in subsection 2.2;
- if the switch occurs the discontinuity generated by the rate limit at $\tau = \varphi(r_V)$, the response maximum will take place at $\phi = \varphi(r_V) - \pi/2$.

The boundary between these two behaviours, shown in Fig.13 by means of a dashed black line,

can be formulated as

$$r_A = \frac{2}{\pi}\sin(\varphi(r_V)). \tag{32}$$

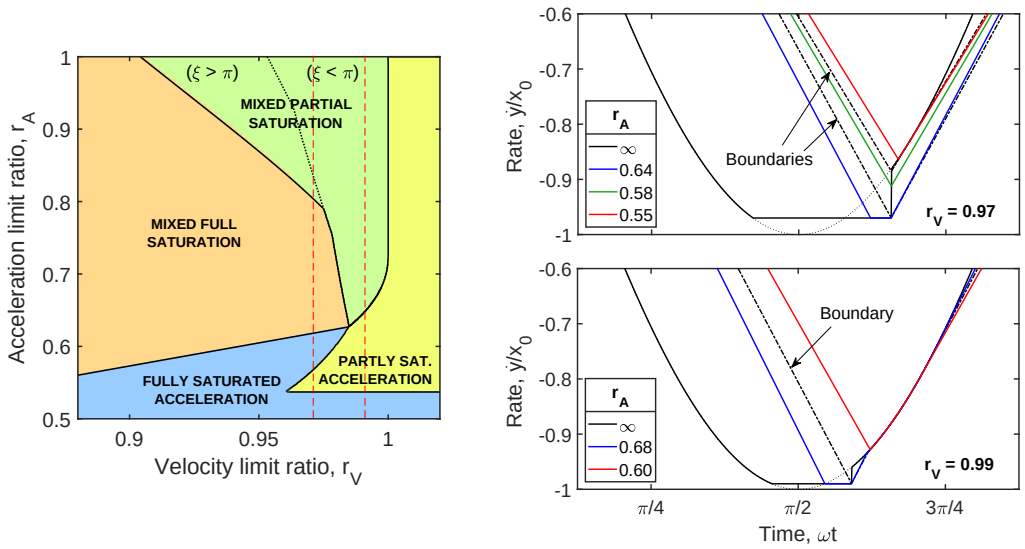

(a) (b)

Figure 12: (**a**) Detail of the saturation regimes in the parameter space $r_V - r_A$ and (**a**) steady-state output rate for varying acceleration limit ratio at $r_V = 0.97$ and $r_V = 0.99$.

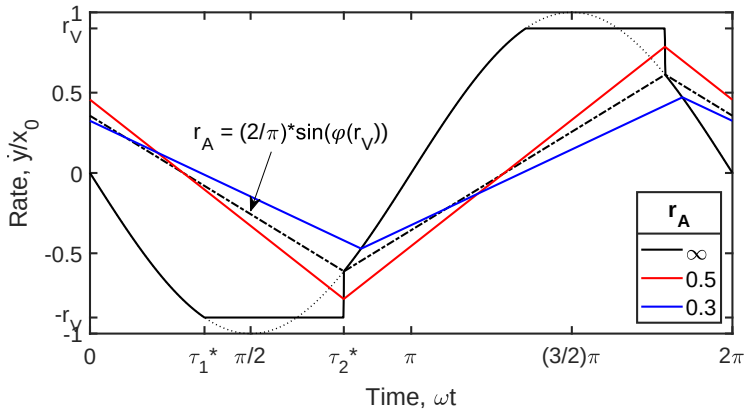

Figure 13: Steady-state output rate for $r_V = 0.9$ and varying acceleration limit ratio.

2.4 Saturation regimes overview

In Fig.14, the boundaries among the saturation regimes, derived in subsections 2.2 and 2.3, are graphically represented in the parameter space defined by r_V and r_A, dividing it in five main regions corresponding to no saturation, partly and fully saturated acceleration, mixed partial and full saturation. Within assumptions of this analysis, rate saturation only is not possible in the presence of an acceleration limit; the full and partial rate saturation regimes, discussed in subsection 2.1, are reported for $r_A \to \infty$ (i.e., when acceleration is not limited). While most properties of such saturation regimes scenario have been discussed above, it is interesting to note the presence of a bifurcation point at $r_V = 0.985$, $r_A = 0.627$. At this point, a small variation in the parameters r_V and r_A can lead to the transition to any of the aforementioned saturation regimes (except to no saturation). In general, it can be stated that there exists a region, characterised by a rate limit ratio close to unity and $r^* \leq r_A \leq r^\wedge$, where several saturation regimes can take place as a result of small variations in r_V or r_A.

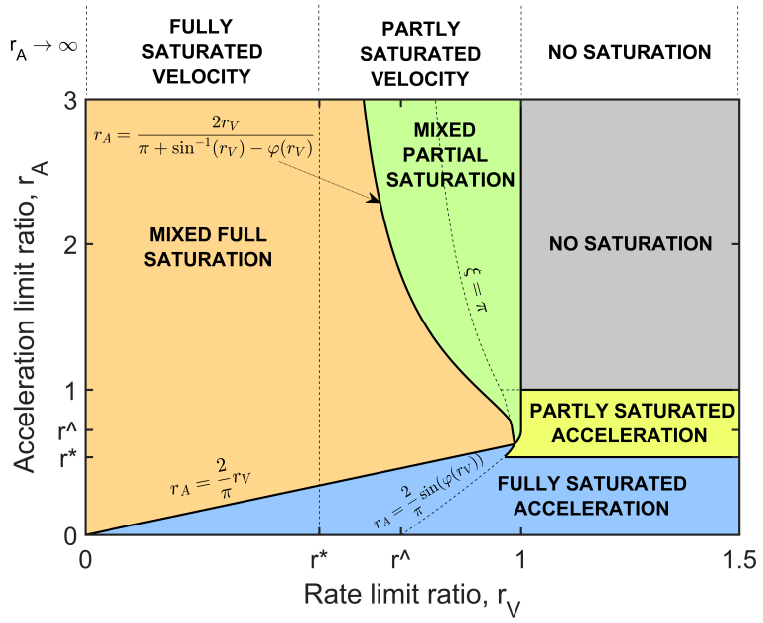

Figure 14: Overview of the saturation regimes determined by rate and acceleration limits in the steady-state actuator response in the parameter space $r_V - r_A$.

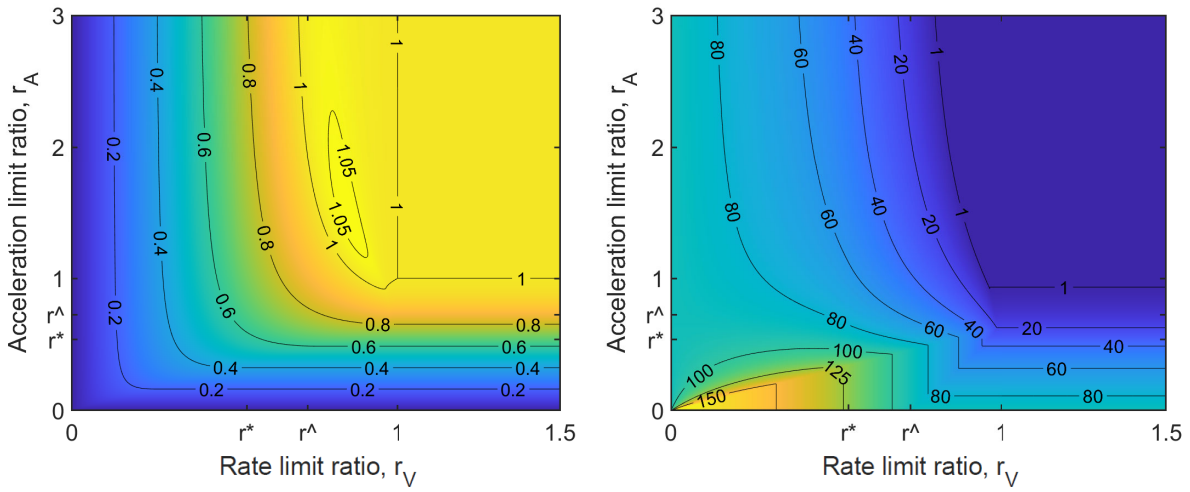

(a) Response amplitude

(b) Phase delay

Figure 15: Non-dimensional response amplitude (**a**) and phase delay (**b**) of the steady-state actuator response for varying rate and acceleration limit ratios.

An overview of the response amplitude and phase delay obtained for varying r_V and r_A is provided in Figs.15a and b, respectively. It can be observed that, despite the fact that these values have been derived by using different formulas across the different saturation regimes, no discontinuities can be observed in these plots. As shown in Fig.15a, the non-dimensional response amplitude gradually increases from zero (when either r_V or r_A tends to zero) to the unitary value observed in the absence of saturation. It is noteworthy that, in mixed partial saturation regime, the response amplitude can exceed that of the sinusoidal input, leading to overshooting. However, the extent of this phenomenon is limited, since the non-dimensional output amplitude has been observed to never exceed 1.06 across the investigated parameter space. The phase delay evolution, in Fig.15b, also presents a gradual increase from zero (when no saturation occurs) to higher values determined by the rate and acceleration limits. While

it has already been observed (see Figs.3a and 7b) the phase delay determined by r_V and r_A, separately, can reach a maximum of 90 degrees, notably higher values are observed in full acceleration regime for $0 < r_V \leq r^*$. In fact, in this region, the phase delay sharply increases reaching a maximum of 180 degrees when both limit ratios tend to zero.

3 ANALYTICAL FORMULATION OF DESCRIBING FUNCTIONS

In this section, sinusoidal describing functions are analytically derived for rate- and acceleration-limited systems. Describing functions can be defined as the ratio between the fundamental harmonic component (first term of the Fourier series) of output and input signals. These functions can be used as a nonlinear extension of the linear concept of transfer function to analyse the behaviour of nonlinear systems behaving as low-pass filters [7], such as those including rate and/or acceleration limits. In fact, even when non-sinusoidal inputs are considered, these systems can effectively suppress higher harmonics, rendering acceptable the approximation introduced with the use of quasi-linear describing functions. The describing function of the rate limit, already introduced in several publications (see, e.g., [1, 9, 20]), will be derived in subsection 3.1 to support the following discussion. The describing functions of the acceleration limit and of combined rate and acceleration limits, whose analytical formulations have not been previously derived to the best of the authors' knowledge, will be introduced in subsections 3.2 and 3.3, respectively. The saturation regimes scenario obtained in the previous section will be used here to determine the frequency ranges where each saturation regime occurs.

3.1 Rate limit

In order to derive the describing function N_V of the rate limit, let us first determine in which frequency range this nonlinearity is active. Based on Eq.(3), it can be deduced that the actuator's response will be unaffected by the presence of the rate limit for angular frequencies smaller or equal to

$$\omega_V = \frac{R_V}{x_0}, \tag{33}$$

where ω_V will be referred to as *onset frequency* of the rate limit, and represents the value of ω such that $r_V = 1$. Similarly the transition from partial to full saturation will take place at higher frequencies when $r_V = r^*$, i.e., when

$$\frac{\omega^*}{\omega_V} = \frac{1}{r^*} \cong 1.862, \tag{34}$$

as also discussed in [1, 14]. In summary, no saturation occurs for $(\omega/\omega_V) \leq 1$, partial rate saturation occurs for $1 < (\omega/\omega_V) < (1/r^*)$ and full rate saturation occurs for $(\omega/\omega_V) \geq (1/r^*)$.

Let us now determine the analytical expression of the rate limit describing function in these three frequency ranges. While the describing function is trivially unitary for $\omega \leq \omega_V$, the analytical formulation in full rate saturation regime can be determined as the ratio between the main harmonic components of the triangle wave response introduced in Sect. 2.1 and of the sinusoidal input. Considering the triangle wave amplitude, equal to $(\pi/2)r_V$ under unitary sinusoidal input, and the phase delay provided by Eq.(12), the describing function can be written here as

$$N_V(r_V) = \frac{4}{\pi} r_V e^{-j\cos^{-1}\left(\frac{\pi}{2}r_V\right)}. \tag{35}$$

It is worth noting that the above expression of the describing function only depends on the rate limit ratio, or on the ratio (ω/ω_V) if the equation is expressed in terms of the angular frequency.

An analytical expression can also be similarly derived in partial saturation regime, although cubic spline interpolation is often used to reconstruct the function N_V in the corresponding frequency range (see, e.g., [1, 9]). The formulation derived by Roman and Ponce in [20] for partial saturation regime, rewritten according to the notation proposed in this paper, reads as

$$\mathrm{Re}\left\{N_V\left(r_V\right)\right\} = \frac{1}{\pi}\Bigg\{\pi + \sin^{-1}(r_V) - \varphi(r_V) + r_V\sqrt{1-r_V^2} + \frac{1}{2}\sin(2\varphi(r_V)) - 2r_V\cos(\varphi(r_V))\Bigg\} \quad (36)$$

$$\mathrm{Im}\left\{N_V\left(r_V\right)\right\} = \frac{1}{\pi}\left[r_V - \sin(\varphi(r_V))\right]^2. \quad (37)$$

The resulting describing function, accounting for full, partial and no saturation regimes, is represented in Fig.16. Bode and phase angle plots of N_V are plotted as a function of the normalised frequency $(\omega/\omega_V) = (1/r_V)$, therefore holding for any value of the rate limit R_V and of input amplitude x_0. It can be observed that, after a gradual decrease occurring in the partial rate saturation frequency range, the gain is reduced at -20dB/decade in full rate saturation, thus confirming the low-pass filter behaviour of the rate limit.

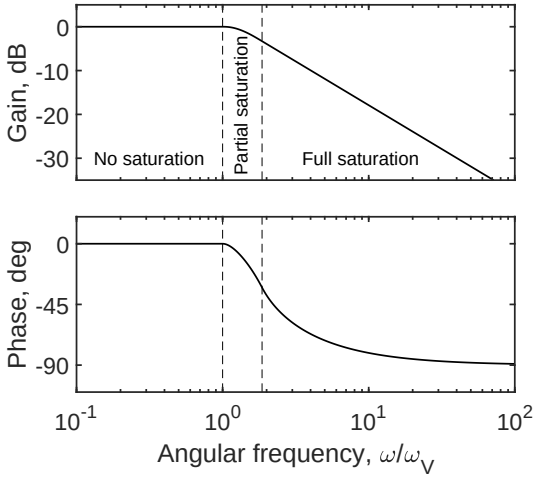

Figure 16: Bode and phase plots of the describing function N_V of the rate limit nonlinearity.

3.2 Acceleration limit

The describing function of the acceleration limit can be determined with the same procedure described above for the rate limit. Let us first introduce the onset frequency of the acceleration limit as

$$\omega_A = \sqrt{\frac{R_A}{x_0}}, \quad (38)$$

so that $\omega = \omega_A$ when $r_A = 1$ and, consequently, $r_A = (\omega_A/\omega)^2$. The derivation of the describing function N_A can be simplified by noting that the steady-state output rate (Fig.4) presents the same evolution as the rate-limited actuator output position (Fig.1), with a phase lead of $\pi/2$, which implies that

$$jN_A(r_A) = e^{j\frac{\pi}{2}}N_V(r_V), \quad (39)$$

and therefore

$$N_A(r_A) = N_V(r_V). \quad (40)$$

It can thus be concluded that N_A will have the same analytical expression as N_V (see Eqs.(35)-(37)) if only r_A is replaced to r_V. As a result, the behaviour of the acceleration limit describing function, represented in Fig.17, is very similar to that described for N_V, with two main notable differences. The Bode plot reveals that the gain is reduced at -40dB/decade in full acceleration saturation regime, as opposed to the -20dB/decade slope observed when full rate saturation occurs. In fact, due to the r_A dependence on ω^2, the acceleration limit has a stronger effect on the actuator output at high frequencies compared to the rate limit. In the same figure, the phase angle is also decreased with a higher rate by the acceleration limit; however, both rate and acceleration limits lead to a phase angle of -90 degrees for $\omega \to \infty$.

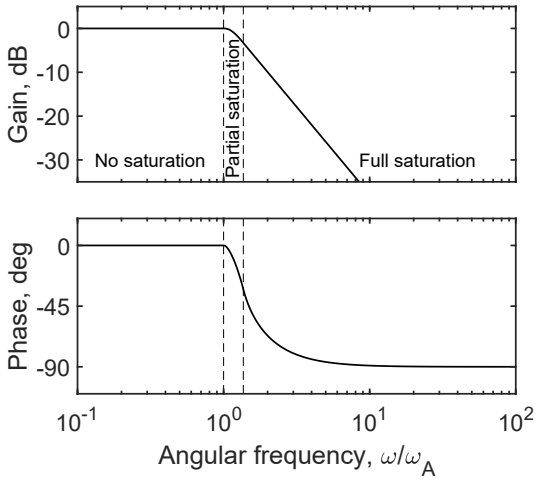

Figure 17: Bode and phase plots of the describing function N_A of the acceleration limit nonlinearity.

3.3 Combined rate and acceleration limit

In this subsection, analytical formulations for the describing function N_{VA} of combined rate and acceleration limits are derived based on the findings presented in Sect.2.3. When $r_V \geq 1$, the output signal is not affected by the rate limit, and therefore the formulations provided in Eqs.(35)-(37) can be referred to for full and partial acceleration saturation regimes, after the position in Eq.(41)is applied. For partial acceleration saturation, it has been shown in Sect.2.3.3 that the response amplitude and phase are unaffected by the rate limit even if this type of saturation occurs for $r_V < 1$, so the above equations can still be used to derive N_{VA} in the corresponding frequency range. For the remaining saturation regimes, analytical formulations of the describing function are provided in what follows for $r_V < 1$.

3.3.1 Full acceleration saturation regime

Based on the results discussed in Sect.2.3, it can be stated that, in full acceleration saturation regime, the steady-state response is a triangle wave of amplitude $(\pi/2)r_A$, regardless of the rate limit value. Conversely, the phase delay generally depends on both r_V and r_A, consistently with the formulations derived in Sect. 2.3.3. While the amplitude of the describing function can be determined by Eqs.(35) and (41) as

$$|N_{VA}(r_V, r_A)| = \frac{4}{\pi} r_A, \tag{41}$$

the phase of this function coincides with the phase delay evaluated in Sect.2, due to the symmetry of the steady-state response, reading as

$$\angle N_{VA}(r_V, r_A) = \begin{cases} \cos^{-1}\left(\frac{\pi}{2} r_A\right) & \text{if } r_A \geq \frac{2}{\pi}\sin(\varphi(r_A)) \\ \varphi(r_V) - \frac{\pi}{2} & \text{if } r^* < r_A < \frac{2}{\pi}\sin(\varphi(r_A)) \\ \frac{\pi}{2} + \cos^{-1}\left(\frac{\pi}{2} r_V\right) & \text{if } r_A \geq r^*. \end{cases} \tag{42}$$

3.3.2 Mixed full saturation regime

In mixed full saturation regime, the actuator output rate is a trapezoidal wave of amplitude r_V and linear traits with rate equal to $\pm r_A$, as shown in Fig.8. The amplitude of the describing function can therefore be easily derived as

$$|N_{VA}(r_V, r_A)| = \frac{4}{\pi} r_A \sin\left(\frac{r_V}{r_A}\right). \tag{43}$$

The symmetry of the steady-state response allows, also in this case, for the evaluation of describing function phase as the phase delay provided in Sect.3.1. From Eqs.(20) and (27), it is possible to write

$$\angle N_{VA}(r_V, r_A) = \begin{cases} \varphi(r_V) + \frac{r_V}{r_A} - \pi & \text{if } r_A > r^* \\ \frac{r_V}{r_A} + \cos^{-1}\left(\frac{\pi}{2} r_V\right) & \text{if } r_A \leq r^*. \end{cases} \tag{44}$$

It is worthwhile underlining that the above equations reduce to Eqs.(41) and (42) for $(r_V/r_A) = (\pi/2)$, i.e., in correspondence of the boundary expressed by Eq.(21), warranting continuity between mixed and acceleration-only full saturation regimes.

3.3.3 Mixed partial saturation regime

The procedure for evaluating the describing function N_{VA} in mixed partial saturation regime cannot be simplified as in fully saturated regimes, not only due to the complex patterns of the actuator output, but also due to the absence of any symmetry properties besides antiperiodicity. This implies that, in general, the maxima (and minima) of the main harmonic component of the response do not coincide with its actual peaks; therefore, the phase angle of N_{VA} differs from the phase delay determined in Sect.2.3. In this case, the derivation of the describing function can only be carried out through a full evaluation of the Fourier coefficients of the first harmonic component of the signal. However, the calculation can be notably simplified by referring to the actuator output acceleration rather than the output position, as detailed in the following equation:

$$N_{VA}(r_V, r_A) = \frac{2}{\pi x_0}\int_{t_1^*}^{t_1^*+\pi} y(t) e^{j\omega t} dt = -\frac{2}{\pi\omega^2 x_0}\int_{t_1^*}^{t_1^*+\pi} \ddot{y}(t) e^{j\omega t} dt = -\frac{2}{\pi}\int_{\tau_1^*}^{\tau_1^*+\pi} \bar{y}''(\tau) e^{j\tau} d\tau. \tag{45}$$

In the above formulation, the half period included between $\tau_1^* = \sin^{-1}(r_V)$ (the starting point of the rate saturation) $\tau_1^* + \pi$ is considered for mathematical convenience. In the parameter space regions where, within mixed partial saturation regime, the acceleration limit only leads to

the saturation of the acceleration peaks generated by rate discontinuities (i.e., for $\xi \geq \pi$ and for $\xi < \pi$ with $r_A \geq 1$), Eq.(45) reduces to

$$N_{VA}(r_V, r_A) = -\frac{2}{\pi}\left[\int_{\varphi(r_V)}^{\xi} r_A e^{j\tau} d\tau - \int_{\xi}^{\tau_1^*+\pi} \cos(\tau) e^{j\tau} d\tau\right] \tag{46}$$

and yields

$$\begin{aligned}\mathrm{Re}\left\{N_{VA}\left(r_V, r_A\right)\right\} = \frac{1}{\pi}\Bigg\{&\pi + \sin^{-1}(r_V) - \xi + r_V\sqrt{1-r_V^2} \\ &-\frac{1}{2}\sin(2\xi) - 2r_A\big[\sin\xi - \sin(\varphi(r_V))\big]\Bigg\}\end{aligned} \tag{47}$$

$$\mathrm{Im}\left\{N_{VA}\left(r_V, r_A\right)\right\} = \frac{1}{\pi}\left\{r_V^2 - \sin^2\xi + 2r_A\big[\cos\xi - \cos(\varphi(r_V))\big]\right\}. \tag{48}$$

Differently, when the acceleration limit also leads to the saturation of the sinusoidal signal (i.e., for $\xi < \pi$ with $r_A < 1$), Eq.(45) leads to

$$\begin{aligned}N_{VA}(r_V, r_A) = -\frac{2}{\pi}\Bigg[&\int_{\varphi(r_V)}^{\xi} r_A e^{j\tau} d\tau - \int_{\xi}^{\cos^{-1}(-r_A)} \cos(\tau) e^{j\tau} d\tau \\ &+ \int_{\cos^{-1}(-r_A)}^{\varphi(r_A)+\frac{\pi}{2}} r_A e^{j\tau} d\tau - \int_{\varphi(r_A)+\frac{\pi}{2}}^{\tau_1^*+\pi} \cos(\tau) e^{j\tau} d\tau\Bigg],\end{aligned} \tag{49}$$

from which

$$\begin{aligned}\mathrm{Re}\left\{N_{VA}\left(r_V, r_A\right)\right\} = \frac{1}{\pi}\Bigg\{&\frac{\pi}{2} + \sin^{-1}(r_V) - \varphi(r_A) + \cos^{-1}(r_A) - \xi + r_V\sqrt{1-r_V^2} \\ &+r_A\sqrt{1-r_A^2} + \frac{1}{2}\big[\sin(2\varphi(r_A)) - \sin(2\xi)\big] - 2r_A\big[\sin\xi - \sin(\varphi(r_V)) + \cos(\varphi(r_A))\big]\Bigg\}\end{aligned} \tag{50}$$

$$\begin{aligned}\mathrm{Im}\left\{N_{VA}\left(r_V, r_A\right)\right\} = \frac{1}{\pi}\Big\{&r_V^2 + r_A^2 - \sin^2\xi + \sin^2(\varphi(r_A)) \\ &+2r_A\big[\cos\xi - \cos(\varphi(r_V)) - \sin(\varphi(r_A))\big]\Big\}.\end{aligned} \tag{51}$$

3.4 Overview for varying rate and acceleration limit

The analytical formulations derived in this section for the describing function N_{VA} enable a full description of the dynamic behaviour of an actuator with combined rate and acceleration limits for varying input frequencies. While it has been shown that N_{VA} can be expressed as a function of the rate and acceleration limit ratios, it is also convenient, in order to determine the frequency ranges where different saturation regime occurs, to derive a relationship between these two quantities as

$$r_A = \frac{R_A x_0}{R_V^2} r_V^2 = \eta_{VA} r_V^2, \tag{52}$$

introducing η_{VA} as a characteristic parameter of the combined rate and acceleration limits. In Fig.18, the curves defined by Eq.(52) are represented in the parameters space $r_V - r_A$, with arrows pointing towards the direction of increasing frequency ω. Observing the intersection of these characteristic curves with the boundaries among the saturation regimes, the following can be deduced:

- if $\eta_{VA} \geq 1$, the onset of nonlinear behaviour is driven by the rate limit and occurs when $r_V = 1$. For $\omega > \omega_V$, the actuator will go through partial and full mixed saturation, and eventually will operate in full saturated acceleration regime as $\omega \to \infty$;
- if $0.646 < \eta_{VA} \leq 1$, the onset of the nonlinearity is driven by the acceleration limit, occurring at $r_A = 1$, while partial acceleration saturation occurs for $\omega_V < \omega < \omega_A$. Starting from $\omega = \omega_V$, the actuator behaviour will be the same as for $\eta_{VA} \geq 1$;
- if $\eta_{VA} \leq 0.646$, rate saturation can never occur, independently of the input frequency. After the nonlinearity activation at $\omega = \omega_A$, a transition from partial to full acceleration saturation will occur at $\omega = \omega_A / r^*$.

The angular frequencies corresponding to the regime transitions can be evaluated from the intersection between the characteristic curves of the combined rate and acceleration limits and the boundaries represented in Fig.18, and the analytical formulations derived in this section for the describing functions can then be applied in the corresponding frequency ranges.

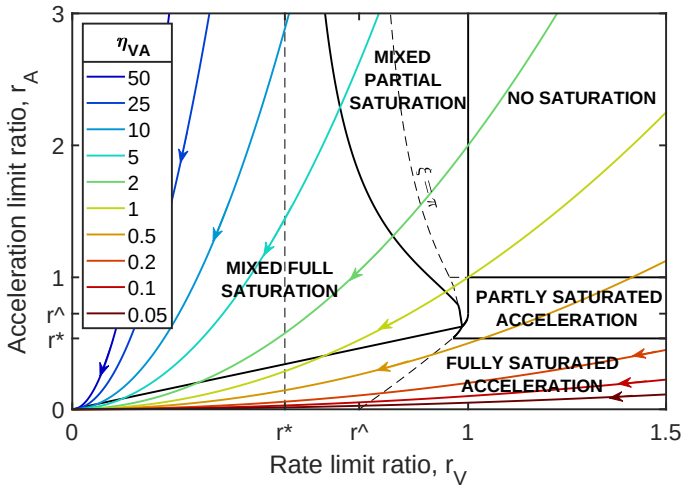

Figure 18: Characteristic curves of combined rate and acceleration limits in the parameter space $r_V - r_A$ for varying η_{VA}. The arrows indicate the direction of increasing angular frequencies.

The resulting describing functions N_{VA} are plotted in Fig.19 for varying η_{VA}; in this figure, the describing function of the rate limit ($\eta_{VA} = \infty$) is also represented as a limit case. The Bode plots clearly show the low-pass filter behaviour induced by the rate and acceleration limits. As discussed above, in the presence of a finite acceleration limit, full acceleration saturation regime always occurs for $\omega \to \infty$; therefore, a gain reduction of 40dB/decade is observed at high frequencies for any η_{VA}. Actuators characterised by large values of η_{VA} behave very similarly to systems with acceleration limit only, while full and partial mixed saturation regimes occur in more and more extended frequency ranges as η_{VA} is decreased, until the behaviour of a rate-limited system is asymptotically recovered.

A very different scenario emerges from the phase angle plot in Fig.19. In this figure, it can be observed that, for combined rate and acceleration limits, the phase angle tends to -180 degrees for $\omega \to \infty$, for any value of η_{VA}, differently from the behaviour observed for systems with rate or acceleration limit only, where the asymptotic values at high frequencies is equal to -90 degrees. When the rate limit is the dominating nonlinearity ($\eta_{VA} > 1$), the phase angle gradually decreases for increasing frequency across the partial and full mixed saturation regimes. However, a sudden change in behaviour is observed when the transition from mixed to acceleration only full saturation regimes occurs; here, an angular point can be observed. In system dominated by the acceleration limit ($\eta_{VA} < 1$), the phase angle first gradually decreases towards

-90 degrees across partial saturation regimes and even full acceleration saturation regime as long as $r_V > r^*$. However, when $r_V = r^*$, another nonsmooth change can be observed in this pattern. Following this angular point, all curves follow the same decreasing pattern towards the asymptotic -180 degrees value; in fact, as shown in Eq.(22), in this saturation regime the phase angle only depends on the rate limit ratio (or, equivalently, on the normalised frequency ω/ω_V). The described phase angle patterns emphasise that cubic spline interpolation, often considered for to address the describing function in partial saturation regime for the rate limit, would lead to misleading results if used in the presence of combined rate and acceleration limits.

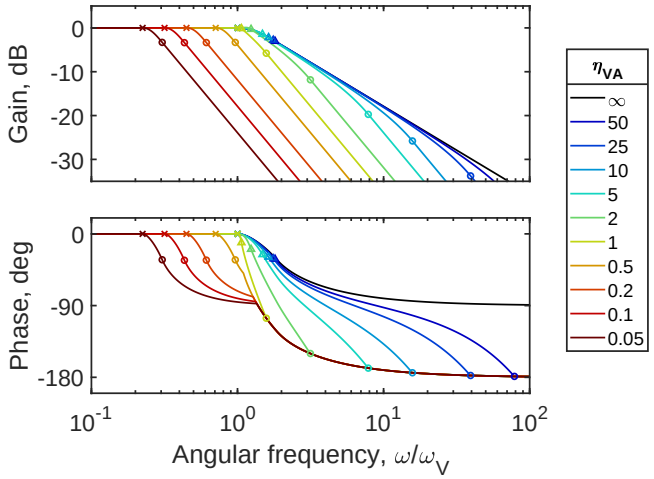

Figure 19: Bode and phase plots of the describing function N_{VA} of combined rate and acceleration limits for varying ratio η_{VA}. Cross markers represent the onset points, triangle markers the transition to full mixed saturation and circle markers the transition to fully saturated acceleration.

4 APPLICATION TO AN AEROSERVOELASTIC MODEL FOR GUST LOAD ALLEVIATION

In this section, the analytical describing functions derived in Sect.3 are applied to the investigation of the nonlinear effects introduced by actuator rate and acceleration limits in the dynamic response of a full aeroservoelastic model. The model considered here as a case-study is an aeroservoelastic wing model developed for gust load alleviation (GLA) purposes, as described in subsection 4.1. An analytical approach for the application of the describing functions to the dynamic analysis of this system is proposed in subsection 4.2, while results are presented in subsection 4.3.

4.1 Model description and control design

The aeroservoelastic wing model considered in this section as a case-study has been developed by the Netherlands Aerospace Center (NLR) within the Clean Aviation UpWing project, and consists of a linear state-space model of 96 states able to describe the wing dynamics with unsteady aerodynamics in response to commands and to gust disturbances. Such a high-order model is not directly applicable for control design purposes because of its high demands on onboard computational loads. Therefore, model order reduction has been performed using the balanced truncation method.

Figure 20 shows a sensitivity analysis on the model reduction order. In this analysis, the aeroelastic model is excited by a 1-cos gust with a frequency of 40 Hz and a magnitude of 4.25 m/s (gust input angle of attack equals 0.9682 degrees). Simulation results show that the gust frequency and magnitude have limited influences on the sensitivity analysis. Regarding the se-

lected gust case, the trend of the root mean square values of the differences between the full and reduced-order models is shown in Fig.20a. Three values are tracked: the wing root shear force, the wing root bending moment, and the wing tip vertical acceleration. Based on this sensitivity analysis, the reduced model order is selected as 35, leading to the differences between the full and reduced order models as rms$(e(F_z))$=0.5904, which is only 0.32% of rms(F_z). rms$(e(M_x))$=0.8290, which is only 0.58% of rms(M_x). The eigenvalue comparisons between the full and reduced order models are also depicted in Fig.20b, showing that the reduced-order model agrees well with the original one in the low frequency range.

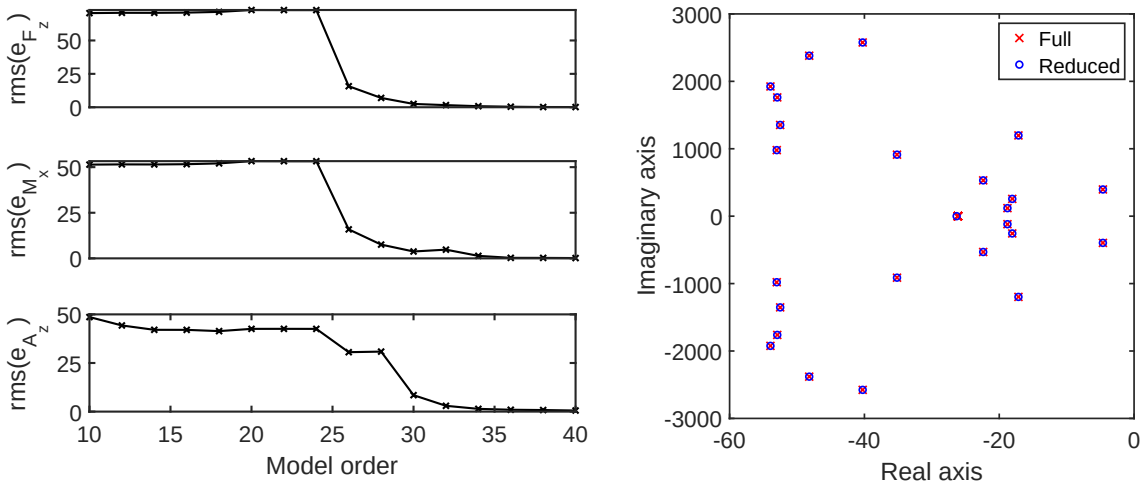

(a) Sensitivity analysis

(b) Eigenvalue comparisons.

Figure 20: Model order reduction for the aeroservoelastic wing model.

A controller has been designed based on the above reduced order linear state-space model for GLA purposes, with primary focus on the wing root bending moment. For simplicity, it is assumed that only the outboard aileron of the wing is used for GLA in this study. The first aeroelastic mode of the wing exhibits a relatively high frequency, approximately equal to 19.7 Hz. Therefore, it becomes essential to consider the actuator bandwidth for controller design. The reduced order model has then been augmented with the dynamics of a first-order actuator with a bandwidth of 90 rad/s (corresponding to about 14.3 Hz). It is noteworthy that the bandwidth value is the only actuator property known to the controller. All other imperfections, uncertainties and nonlinearities, including rate and acceleration limits, are not known by the controller and are expected to be accommodated by the controller's inherent robustness.

The control approach adopted in this study is the Linear Quadratic Regulator (LQR), an optimal control strategy for systems characterized by linear dynamics and quadratic cost functions. It aims to minimize a cost function that balances state deviation and control effort. The solution involves solving algebraic Riccati equations [21]. The control cost function is given by $J = \int_0^\infty (x(t)^T Q x(t) + u(t)^T R u(t))\,\mathrm{d}t$. The relative value between Q and R reflects a trade-off in between performance and control efforts. Without loss of generality, in this study, the Q matrix is simply chosen as an identity matrix with a scale of 10^3, while R is a single value of 200.

A block diagram of the linear aeroservoelastic model is depicted in Fig.21. The actuator is here modelled as first-order system described by the linear transfer function

$$G_a(s) = \frac{\omega_n}{s + \omega_n}, \tag{53}$$

where $\omega_n = 90$ rad/s. The actuator is placed in a feedback loop along with the aeroelastic system and the LQR controller; plant and controller are described by the transfer function $G_{pc}(s)$. In order to analyse the nonlinear dynamic effects caused by actuator rate and acceleration limits, it is necessary to evaluate the frequency response of this feedback loop including the describing function N_{VA}, as detailed in what follows.

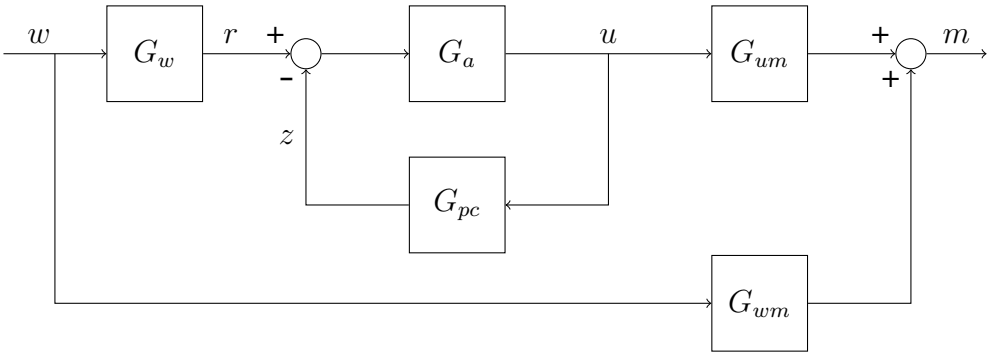

Figure 21: Block diagram of the UpWing aeroservoelastic wing model for gust load alleviation.

4.2 Describing function of a closed-loop system

An approach for the evaluation of the equivalent describing function of a closed-loop system including a rate limit nonlinearity has been proposed by Gilbreath [1]. In this subsection, Gilbreath's approach is extended to also deal with acceleration limits and applied to the closed-loop of the controlled aeroservoelastic model described above.

Let us now introduce in the model the actuator rate and acceleration limits by means of the describing function N_{VA}, whose analytical formulation has been derived in Sect. 3. The resulting closed-loop system is illustrated in Fig.22. The proposed procedure consists of two main steps, i.e., the evaluation of the onset frequency of the nonlinear behaviour and the derivation of an equivalent describing function for the entire feedback loop.

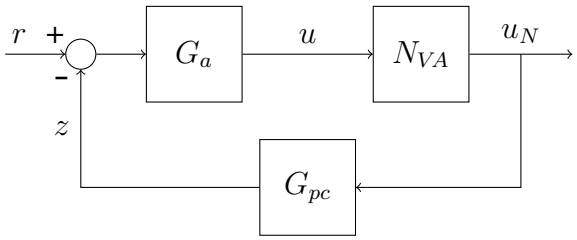

Figure 22: Actuator-plant-controller feedback loop of the UpWing aeroservoelastic wing model accounting for actuator nonlinearity.

For the first step, a graphical and analytical procedure is here proposed as an extension of that proposed by Gilbreath for rate-limited systems [1]. If the rate limit is considered as the only actuator nonlinearity, the feedback loop behaves linearly for $r_V \geq 1$, and the onset frequency $\tilde{\omega}_V$ of the nonlinear behaviour can be obtained from the condition $r_V = 1$. Considering the definition of r_V from Eq.(5), $\tilde{\omega}_V$ can be determined as a solution of the equation

$$r_0 \left| \frac{u}{r}(j\tilde{\omega}_V) \right| = \frac{R_V}{\tilde{\omega}_V}, \tag{54}$$

where the left-hand side corresponds to the amplitude of the rate limit input u in the feedback

loop. Since the closed-loop system behaves linearly for $\omega \leq \tilde{\omega}_V$, the presence of the nonlinear element can be disregarded when evaluating the transfer function between u and r in the above equation, which therefore reads as

$$\frac{u}{r}(\omega) = \frac{G_a(\omega)}{1 + G_a(\omega)G_{pc}(\omega)}. \tag{55}$$

In Fig.23, the left-hand side of Eq.(54) is represented by the black curve, while the right-hand side corresponds to the grey straight line, characterised by a slope of -20 dB/decade and crossing the 0 dB line at $\omega = R_V$. The closed-loop rate limit onset frequency graphically results from the intersection of these lines.

If the actuator acceleration limit R_A is considered in place of the rate limit, the closed-loop onset frequency of the nonlinearity can be similarly determined from the equation

$$r_0 \left| \frac{u}{r}(j\tilde{\omega}_A) \right| = \frac{R_A}{\tilde{\omega}_A^2}, \tag{56}$$

which is obtained from the condition $r_A = 1$. The right-hand side of the above equation is graphically represented by a straight line with slope -40 dB/decade crossing the 0 dB line at $\omega = R_A$, as shown in Fig.23 for different values of the acceleration limit.

If actuator rate and acceleration limits are both taken into account, the closed-loop onset frequency of the actuator nonlinearity will be the smallest value between $\tilde{\omega}_V$ and $\tilde{\omega}_A$, consistently with the findings presented in Sect.3.4. The describing function of the feedback loop will then be characterised by two main behaviours: below the closed-loop onset frequency, the system will still behave linearly; above this frequency, the system will be affected by rate and acceleration limits and will exhibit a nonlinear behaviour, which will be characterised in what follows.

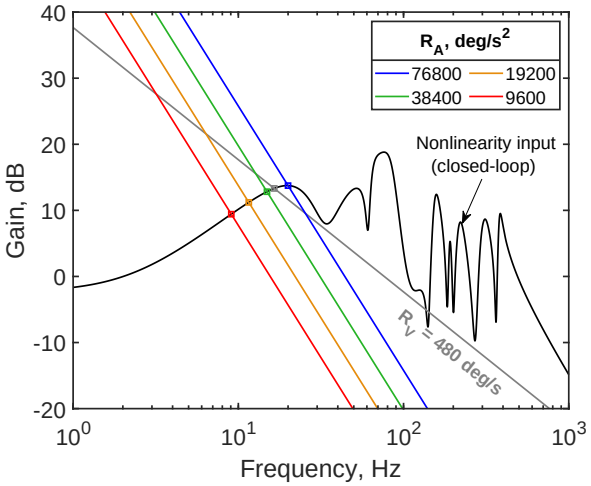

Figure 23: Graphic determination of the closed-loop onset frequency in the presence of combined rate and acceleration limits.

The second step of the procedure consists of the evaluation of the equivalent describing function for the entire feedback loop, aiming at determining the effect of the nonlinearity on its frequency response. Referring to Fig.22, let us assume that the feedback loop input signal can be represented in the complex time domain as

$$r(t) = r_0 e^{j\omega t}. \tag{57}$$

Then, the input signal of the nonlinear element can be written as

$$u(t) = u_0 e^{j(\omega t + \phi_0)}. \tag{58}$$

For $\omega > \min\{\tilde{\omega}_V, \tilde{\omega}_A\}$, i.e., after the onset of the combined rate and acceleration limits, the signal $u(t)$ is also affected by the nonlinearity, due to the loop closure. Therefore, the amplitude u_0 and the phase angle ϕ_0 represent two unknown variables of the problem. To determine their values, the following relationship can be considered:

$$(r_0 - Y(\omega))|G_a(\omega)|e^{j\angle G_a(\omega)} = u_0 e^{j\phi_0}, \tag{59}$$

where

$$Y(\omega) = u_0 e^{j\phi_0}|N(\omega, u_0)|e^{j\angle N(\omega,u_0)}|G_{pc}(\omega)|e^{j\angle G_{pc}(\omega)}, \tag{60}$$

leading to the following system of nonlinear equations:

$$\begin{cases} \dfrac{u_0}{|G_a(\omega)|}\cos\phi_1 + u_0|N(\omega, u_0)||G_{pc}(\omega)|\cos\phi_2 = r_0 \\ \dfrac{u_0}{|G_a(\omega)|}\sin\phi_1 + u_0|N(\omega, u_0)||G_{pc}(\omega)|\sin\phi_2 = 0, \end{cases} \tag{61}$$

where $\phi_1 = \phi_0 - \angle G_a(\omega)$ and $\phi_2 = \phi_0 + \angle N(\omega, u_0) + \angle G_{pc}(\omega)$. The unknowns u_0 and ϕ_0 can finally be determined by using, for instance, a nonlinear optimisation algorithm over the frequency range of interest. The closed-loop describing function can be evaluated, at this stage, by using standard linear techniques, resulting in

$$N_c(\omega, r_0) = \frac{|N(\omega, u_0)||G_{pc}(\omega)|u_0}{r_0} e^{j\phi_2}, \tag{62}$$

while the corresponding open-loop describing function can be obtained from the above expression as

$$N_o = \frac{N_c}{1 - N_c}. \tag{63}$$

4.3 Results and discussion

The above procedure has been applied to the aeroservoelastic model from Fig.21, considering the gust input amplitude w_0 = 4.25 m/s, a rate limit equal to 480 deg/s and the acceleration limit values 76800, 38400, 19200 and 9600 deg/s^2. In addition, the case of an actuator with rate limit only ($R_A = \infty$) has also been investigated.

The resulting open-loop equivalent describing functions are reported in Fig.24a, along with the linear open-loop transfer function, which can be derived from its corresponding closed-loop formulation in Eq.(55). The $r_V - r_A$ curves, referring to the actuator nonlinearity input in the feedback loop, are represented in Fig.24b, to identify the saturation regimes occurring in the investigated frequency range (between 1 and 10000 Hz).

Observing the intersections between the nonlinearity input curves and the boundaries corresponding to $r_V = 1$ and $r_A = 1$ in Fig.24b, it is possible to note that the rate limit only drives the nonlinearity onset in the case R_A = 76800 deg/s^2, consistently with the results shown in Fig.23, while the acceleration limit determines the onset point in the remaining three cases. The main nonlinear phenomenon observable in the describing functions is the presence of a jump

discontinuity occurring at a slightly higher frequency than the onset frequency. The presence of this jump was already observed by Gilbreath for rate-limited systems [1], where it is also referred to as *jump resonance*, a well-known phenomenon in nonlinear dynamics (see, e.g., [22]). Fig.24b clearly shows that the jump resonance takes place at the transition from partial to full saturation, independently of which actuator state (velocity, acceleration or both) is saturated. As visible in Fig.24a, the jump consists in a dramatic drop of phase angle, along with a more limited drop in the gain of the describing function. In references [1, 23], it was observed how this jump phenomenon can cause closed-loop system instability, since it pushes the frequency response across the critical point (180 degrees, 0 dB) in the Nichols chart; this will be the object of further investigation. After the jump, the actuator operates in full saturation. If only the actuator rate is limited, full saturation occurs in an extensive frequency range (up to about 1350 Hz), and is then followed by partial saturation and, eventually, no saturation at higher frequency, where the system's response becomes linear again. Conversely, if the actuator acceleration is also limited, full acceleration saturation regime will take place, starting from the phase drop. When $\omega \to \infty$, it has been observed that $r_V \to \infty$, while r_A converges to a small finite value (in the order of 10^3 in the investigated cases). Therefore, the actuator eventually operates in full acceleration saturation regime with

$$r_A > \frac{2}{\pi} \sin(r_V), \tag{64}$$

where, from Eq.(42), the phase angle is approximately equal to -180 degrees for $r_A \cong 0$. In this saturation regime, the gain of the describing function decreases with a slope of -20 dB/decade (the same as observed in the linear case), but strong attenuation is induced by the acceleration limit, rendering negligible the output of the control loop.

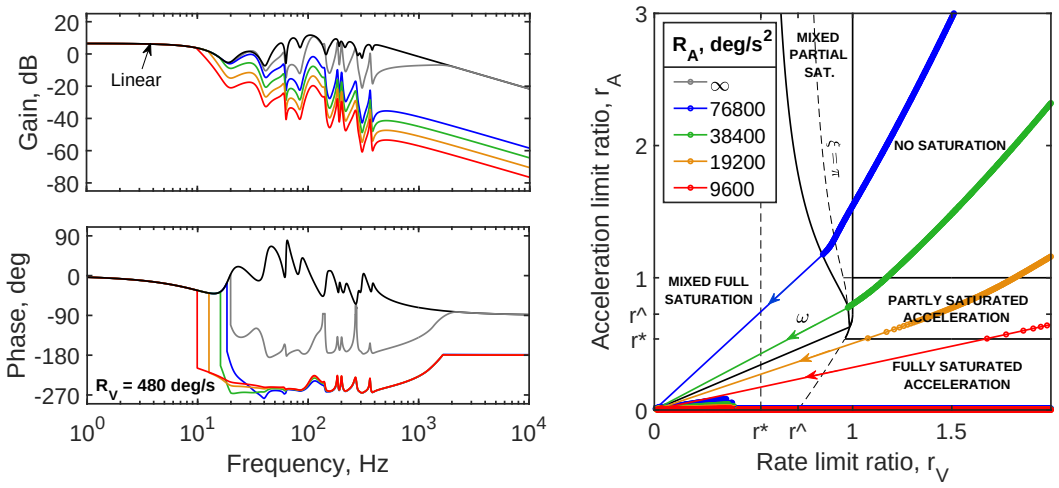

(a) (b)

Figure 24: (**a**) Bode and phase plots of the open-loop equivalent describing function for the actuator-plant-controller loop, for $R_V = 480$ deg/s and varying R_A, and (**b**) characteristic curves of the actuator in the parameter space $r_V - r_A$. The arrows indicate the direction of increasing frequencies.

Finally, the effect of the actuator rate and acceleration limits on the aeroservoelastic system performance for GLA has been investigated by replacing the feedback loop with its equivalent describing function, hence performing a quasi-linear analysis. The frequency response of the wing root bending moment is reported in Fig.25 for the rate limit R_V = 480 deg/s and varying values of R_A. The results are compared to the linear closed-loop case, corresponding to the ideal functioning of the control system in the absence of nonlinear behaviours, and to the linear

system not featuring GLA (i.e., no control loop). As expected, no effects from rate and acceleration limits are observed below the onset frequency, while their effect is generally detrimental in the remaining frequency range. The jump resonance occurs at a slightly higher frequency than the nonlinearity onset and has a strong impact on the system's performance, which degrades even below that observed without GLA after the jump. The worst scenario is represented by the case where only rate limit is considered, since the wing root bending moment is amplified in a wide frequency range, approximately between 11 and 70 Hz. This range also includes the frequency of the first aeroelastic mode of the wing, where load alleviation is most needed. In this context, the actuator acceleration limit appears to have a double effect: on the one hand, it leads to lower onset and jump frequencies, further reducing the effective frequency range of the controller; on the other hand, at higher frequencies, it can limit the detrimental effect of the rate limit by simply rendering the actuator ineffective and reducing the system's behaviour to the open-loop case (no GLA).

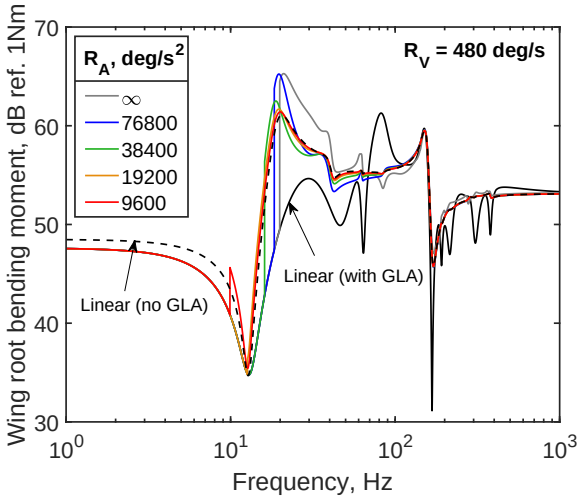

Figure 25: Wing root bending moment frequency response under gust excitation of magnitude 4.2472 m/s: comparison among linear response with and without gust load alleviation, rate-limited actuator and rate- and acceleration-limited actuator with varying acceleration limits.

From the presented analysis, it can be concluded that the designed control system becomes ineffective (or even detrimental) above the partial-to-full saturation transition frequency. The identification of this frequency is therefore essential to define the effective frequency range of the control system, which should at least include the frequencies of those aeroelastic modes for which load alleviation is required.

5 CONCLUSIONS

In this paper, the nonlinear effects introduced by rate and acceleration limits in the actuator response have been analysed. A full overview of the saturation regimes determined by these nonlinearities in the steady-state actuator response to sinusoidal input has been presented, deriving analytically the conditions for the transitions across the different regimes and evaluating the saturation effect on the response amplitude and phase delay. Analytical expressions have also been derived for the sinusoidal describing functions of the rate, acceleration and combined rate and acceleration limits, allowing for a full description of the relationship between actuator input and output in the frequency domain. Finally, the derived describing functions have been applied to the analysis of an aeroservoelastic system to determine the effect of actuator rate and acceleration limits on its gust load alleviation performance.

The investigation of the actuator saturation regimes has shown that several types of steady-state responses can be observed if a rate- and/or acceleration-limited system is subjected to sinusoidal excitation, including different types of partial and full saturation of the actuator rate, acceleration, or both quantities. When rate and acceleration limits are simultaneously applied, strong acceleration limits can conceal the presence of a rate limit, having a leading effect on the response amplitude. However, even when rate saturation is not observed, the rate limit has an important effect on the phase delay, which can therefore be considered as an important metric for rate limit identification from experimental observations. In general, the investigation of the parameter space $r_V - r_A$ defined by the non-dimensional rate and acceleration limit ratios, has revealed that the combined application of these nonlinearities has a major effect on the output phase delay, which can increase up to 180 degrees in the worst-case scenario. This result is also confirmed by the derived describing functions, where this phase angle value is eventually reached at high frequencies, as opposed to the asymptotic value of 90 degrees observed if only one of these actuator nonlinearities is considered. Moreover, while the gain of these describing functions exhibits a typical low-pass filter behaviour, with slope equal to -40 db/decade when the acceleration limit is considered, the phase angle evolution presents more complex patterns, often characterised by the presence of angular points when regimes transitions occur. This phenomenon suggests that the complete analytical formulation of the describing functions derived in this paper should be used when performing stability analysis, since cubic spline interpolation, often considered for partial saturation regimes, could lead to misleading results.

The nonlinear analysis of the aeroservoelastic system considered in this paper as a case-study, has revealed that the nonlinear effects generated by rate and acceleration limit nonlinearities in closed-loop systems can be very significant and have a close connection with the occurrence of the different actuator saturation regimes described in this paper. In particular, jump resonances have been observed in correspondence with the transition from partial to full saturation regimes (independently of whether rate, acceleration or both quantities are saturated). The sudden drop of the response phase angle, along with the reduced output amplitude, can render the actuator ineffective in the presence of rate and acceleration limits at higher frequencies, strongly reducing the gust load alleviation performance of the system. The effective frequency range of the control system is therefore limited by the frequency of this jump resonance. This emphasises the importance of considering rate and acceleration limits in the actuator selection process. Further investigation is required to determine the effect of the nonlinear jump phenomenon on the dynamic stability of the system.

6 REFERENCES

[1] Gilbreath, G. (2001). Prediction of pilot-induced oscillations due to actuator rate limiting using the open-loop onset point criterion. Tech. rep., Air Force Institute of Technology, Wright-Patterson Air Force Base, OH.

[2] Tang, M., Böswald, M., Govers, Y., et al. (2021). Identification and assessment of a nonlinear dynamic actuator model for controlling an experimental flexible wing. *CEAS Aeronautical Journal*, 12, 413–426. doi:10.1007/s13272-021-00504-y.

[3] Theis, J., Pfifer, H., and Seiler, P. (2016). Robust control design for active flutter suppression. In *AIAA Atmospheric Flight Mechanics Conference*. p. 1751. doi: 10.2514/6.2016-1751.

[4] Pusch, M., Ossmann, D., and Luspay, T. (2019). Structured control design for a highly flexible flutter demonstrator. *Aerospace*, 6(3), 7. doi:10.3390/aerospace6030027.

[5] McRuer, D. (1997). *National Research Council: Aviation Safety and Pilot Control: Understanding and Preventing Unfavorable Pilot-Vehicle Interactions*. Washington, DC: The National Academies Press.

[6] Duda, H. (1998). Flight control system design considering rate saturation. *Aerospace Science and Technology*, 2(4), 265–275. doi:10.1016/S1270-9638(98)80004-7.

[7] Fielding, C. and Flux, P. (2003). Non-linearities in flight control systems. *The Aeronautical Journal*, 107(1077), 673–696. doi:10.1017/S0001924000013543.

[8] Tang, M., Böswald, M., Govers, Y., et al. (2019). Identification and assessment of a nonlinear dynamic actuator model for gust load alleviation in a wind tunnel experiment. In *Deutscher Luft- und Raumfahrtkongress*.

[9] Yuan, J., Fei, S., and Chen, Y. (2020). Compensation strategies based on bode step concept for actuator rate limit effect on first-order plus time-delay systems. *Nonlinear Dynamics*, 99(2), 2851–2866. doi:10.1007/s11071-019-05454-z.

[10] Roberge, J. (1975). *Operational Amplifiers: Theory and Practice*. Wiley & Sons.

[11] Slotine, J.-J. and W., L. (1991). *Applied Nonlinear Control*. Englewood Cliffs, NJ: Prentice-Hall International Editions.

[12] Hanke, D. (1995). Handling qualities analysis on rate limiting elements in flight control systems. In *Flight Vehicle Integration Panel Workshop in Pilot Induced Oscillations, AGARD-AR-335*.

[13] Katayanagi, R. (2001). Pilot-induced oscillation analysis with actuator rate limiting and feedback control loop. *Transactions of the Japan Society for Aeronautical and Space Sciences*, 44(143), 48–53. doi:10.2322/tjsass.44.48.

[14] Duda, H. (1994). Frequency domain analysis of rate limiting elements in flight control systems. Tech. rep., DLR-FB 94-16.

[15] Amato, F., Iervolino, R., Pandit, M., et al. (2000). Analysis of pilot-in-the-loop oscillations due to position and rate saturations. In *Proceedings of the 39th IEEE Conference on Decision and Control*, vol. 4. p. 3564–3569. doi:10.1109/CDC.2000.912258.

[16] Meng, J., Xu, H., and Zhang, J. (2010). A comparison of rate-limit phase compensator to prevent category ii pilot induced oscillations. In *Proceedings of the 8th World Congress on Intelligent Control and Automation*. p. 3872–3877. doi:10.1109/WCICA.2010.5555356.

[17] Alstrom, R., Bollt, E., Marzocca, P., et al. (2012). The application of nonlinear prefilters to prevent aeroservoelastic interactions due to actuator rate limiting. In *Proceedings of the 53rdAIAA/ASME/ASCE/AHS/ASC Structures, Structural Dynamics and Materials Conference*. doi:10.2514/6.2012-1483.

[18] Nakabayashi, Y., Okajima, H., and Matsunaga, N. (2017). Signal limitation filter to satisfy velocity and acceleration constraints for arbitrary input signals. In *Proceedings of the 56th Annual Conference of the Society of Instrument and Control Engineers of Japan*. pp. 1197–1201. doi:10.23919/SICE.2017.8105481.

[19] Tombul, G. (2021). Simultaneous feedforward online command rate limiter filters for existing controllers. *Turkish Journal of Electrical Engineering and Computer Sciences*, 29(5), 2529–2544. doi:10.3906/elk-2007-147.

[20] Román, M. and Ponce, E. (2003). The describing function method accuracy in first order plants with rate-limited feedback. *2003 European Control Conference (ECC), Cambridge, UK*, 1620–1625. doi:10.23919/ECC.2003.7085195.

[21] Lehtomaki, N. and Sandell, N. (1981). Robustness results in linear-quadratic gaussian based multivariable control designs. *IEEE Transactions on Automatic Control*, 75–93. doi:10.1109/TAC.1981.1102565.

[22] Graham, D. and Mc Ruer, D. (1961). *Analysis of Nonlinear Control Systems*. New York: Wiley & Sons.

[23] Yuan, J., Chen, Y., and Fei, S. (2018). Analysis of actuator rate limit effects on first-order plus time-delay systems under fractional-order proportional-integral control. *International Federation of Automatic Control PapersOnLine*, 51(4), 37–42. doi:10.1016/j.ifacol.2018.06.022.

ACKNOWLEDGEMENTS

This research has been performed in the frame of the CONCERTO project (Construction Of Novel CERTification methOds and means of compliance for disruptive technologies), which is funded by the European Community's Clean Aviation Joint Undertaking programme, under Grant Agreement No 101101999. The project started on January 1, 2023.

The aeroservoelastic wing model referred in this work has been developed by the Netherlands Aerospace Center (NLR) the European Community's Clean Aviation programme, under the Grant Agreement 101101974. The UPWing project (Ultra-Performance Wing) is a project funded under the topic Climate, Energy and Mobility, involving 26 partners. The project started on January 1, 2023.

DISCLAIMER

COPYRIGHT STATEMENT